Bulgarian Chemical Communications, Volume 56, Issue 2 (pp. 125-146) 2024 *DOI: 10.34049/bcc.56.2.5626*

Cobalt complexes of pyridine carboxaldehyde Schiff bases as cholinesterase inhibitors and anti-proliferative activity

A. Naseer[1,2], A. Naz Awan[1*], J. Iqbal[3], S. Habib[4], A. Javed[4]

[1] *Department of Pharmaceutical Chemistry, Faculty of Pharmacy and Pharmaceutical Sciences, University of Karachi, Karachi 75270, Pakistan*

[2]*College of Pharmacy – Isra University, Hyderabad, Pakistan*

[3]*Center for Advanced Drug Research, COMSATS University Islamabad, Abbottabad Campus, Abbottabad 22060, Pakistan*

[4]*Healthcare Biotechnology, Atta-ur-Rahman School of Applied Biosciences, National University of Science and Technology, Islamabad, Pakistan*

Received: January 25, 2024; Revised: May 15, 2024

Novel cobalt complexes of pyridine carboxaldehyde were meticulously designed, synthesized, and subsequently screened to assess their broad spectrum of biological potential. Pyridine carboxaldehyde semicarbazone, thiosemicarbazone, and cobalt chloride served as the initial materials, which were subjected to ultrasonication for the synthesis of the cobalt complexes. Characterization of the obtained compounds was conducted using FTIR, ^{1}H-NMR, elemental analysis, and both *in-silico* and *in-vitro* assessments were performed to evaluate their cholinesterase inhibition and anti-proliferative properties. It was found that all synthesized molecules selectively inhibited acetylcholinesterase within a range of IC_{50} values from 0.97±0.02 to 6.47±0.71 µM. Notably, CoRx-1Cl_2 exhibited non-selective inhibition against both acetylcholinesterase and butyrylcholinesterase, with IC_{50} values of 1.91±0.08 and 12.97±2.46 µM, respectively. Subsequent MTT assays and cytotoxic studies were carried out on U-87 and HEK-293 cell lines, revealing that all synthesized compounds were non-toxic to the normal cell line HEK-293. Conversely, cell viability in U-87 cells ranged from 20.93% to 92.9%. These findings suggest that the synthesized cobalt complexes possess a multi-targeting effect and hold potential for use in the management of conditions such as Glioblastoma and Alzheimer's diseases.

GRAPHICAL ABSTRACT

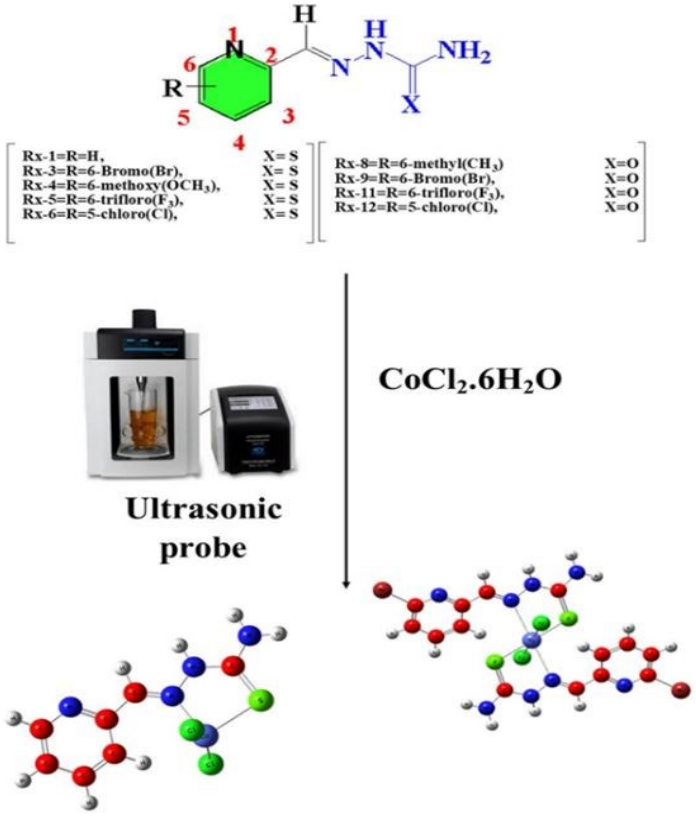

Keywords: Schiff bases; Cobalt complexes; Ultrasonic probe; Cholinesterase inhibition; MTT assay.

* To whom all correspondence should be sent:
E-mail: asia.naz@uok.edu.pk

INTRODUCTION

The enzymes acetylcholinesterase (AChE) and butyrylcholinesterase (BuChE) belong to the class of serine hydrolases [1, 2]. They can hydrolyze acetylcholine (ACh) and a few other choline esters, albeit with varying degrees of relative efficiency. Additionally, cholinesterases may exhibit peptide hydrolysis or aryl acyl amidase activity [3]. In the modern world, conditions such as Alzheimer's disease (AD) and cancer are prevalent and often fatal illnesses, posing significant societal and economic challenges [4, 5]. AD is characterized by the loss of cholinergic neurons, leading to alterations in the concentrations of AChE and BuChE [6, 7], while cancer represents a global health concern due to its unique nature characterized by the uncontrolled growth of abnormal cells [8]. Although cancer research has yielded numerous novel and effective treatments, the drugs currently employed to address these conditions have evident limitations [9, 10].

Improving and stabilizing the symptoms of AD may be achievable by maintaining the level of this essential neurotransmitter in brain tissues [2, 11]. Additionally, acetylcholinesterase (AChE) may play a significant role in cancer development and could potentially serve as a target for treatment, given its involvement in non-neuronal processes such as the regulation of cell proliferation, differentiation, and apoptosis [12]. One possible mechanism linking neurodegeneration and malignancy involves the non-enzymatic binding of AChE to an allosteric site on the nicotinic alpha-7 receptor, which operates at both neuronal and non-neuronal levels. Furthermore, AChE may be crucial for the migration of cancer cells, suggesting a pathway that intersects neurodegeneration and carcinogenesis [13, 14].

Semicarbazone (SC) and thiosemicarbazone (TSC) represent classes of Schiff bases derived from the condensation of aldehydes [15] or ketones with semicarbazide and thiosemicarbazide, respectively, wherein the carbonyl group is replaced by an imine bond. Schiff bases constitute an exceptional category of ligands that demonstrate remarkable coordination modes towards transition metals owing to their diverse array of donor atoms [16, 17]. In the formation of metallic complexes, SC and TSC ligands often coordinate to transition metals through their oxygen, nitrogen, and sulfur donor atoms, adopting either their (N, S) bidentate form or (N, N, S or O, N, S) tridentate form [18, 19]. These complexes may exhibit bioactivities that surpass those of the free ligands, including acting as DNA binding agents [20], antiviral [21], antifungal [22], antimicrobial [23, 24], anticancer [23, 25], SARS-CoV-2 inhibitors [26], inhibitors of topoisomerase IIα [27], and monoamine oxidase-B inhibitors [28], as well as displaying acetylcholinesterase inhibition properties [28, 29].

Previous research [30] has utilized experimental approaches to assess the biological activity of compounds against enzymes. Scientists continuously seek innovative compounds to enhance biological activity, often linking metal atoms and ligand molecules to synthesize novel complexes. Researchers have discovered that these metal complexes exhibit greater biological activity compared to their ligands [31, 32], thereby demonstrating more potent inhibition against enzymes.

In the present study, conventional methods such as sol-gel or thermal degradation for synthesizing complexes have been replaced with ultrasonication. This alternative technique offers several advantages, including cost efficiency, environmental friendliness, and the ability to perform treatments on-site. Specifically, this research focuses on the ultrasound-assisted fabrication of cobalt complexes derived from recently reported pyridine carboxaldehyde semicarbazone and thiosemi-carbazone [33]. These complexes are subsequently examined to assess their inhibitory effect on cholinesterase enzymes, as well as their anti-proliferative effect against both the U-87 cancer cell line and the HEK-293 normal cell line.

RESULTS AND DISCUSSION

The 0.001 molar water/ethanolic solutions of substituted semicarbazone and thiosemicarbazones were added dropwise to a 0.001 molar cobalt chloride solution while keeping it in a high-density ultrasonic probe. Sonication was continued for 30 minutes, after which the product was precipitated out, filtered, washed with ethanol, and dried, then stored in a closed container for further study.

A cobalt complex of pyridine carboxaldehyde thiosemicarbazone was discussed here as an example for spectral studies. The NH peak appeared at 3390 cm^{-1}, indicating the presence of one free primary amino group. Peaks at 1581 cm^{-1} and 837 cm^{-1} were observed for the stretching of C=N and C=S, respectively, which were slightly shifted to lower wavelengths compared to the respective pyridine carboxaldehyde thiosemicarbazone, which exhibited peaks at 1622 cm^{-1} and 877 cm^{-1}. These findings from FTIR suggest the bidentate behavior of pyridine carboxaldehyde thiosemicarbazone, involving the azomethine group (-C=N-) and sulfide group (-C=S-) moieties interacting with the core cobalt metal ions. The ^{1}H-NMR results also

confirmed the FTIR findings. The aromatic ring proton appeared at δ 7.369 (t, 1H), 7.821 (t, 1H), 8.272 (d, 1H), 8.557 (d, 1H), while the CH-N appeared at δ 8.082 (s, 1H), NH appeared at δ 11.642 (s, 1H), and the terminal amine appeared at δ 8.180 (s, 1H).

The solubility study revealed that the obtained complexes are insoluble in diethyl ether, ethanol, and acetonitrile, slightly soluble in chloromethane and carbon tetrachloride, and soluble in DMSO and DMF.

A series of cobalt complexes of pyridine carboxaldehyde semicarbazone and thiosemicarbazone were synthesized according to the details provided in Scheme 1.

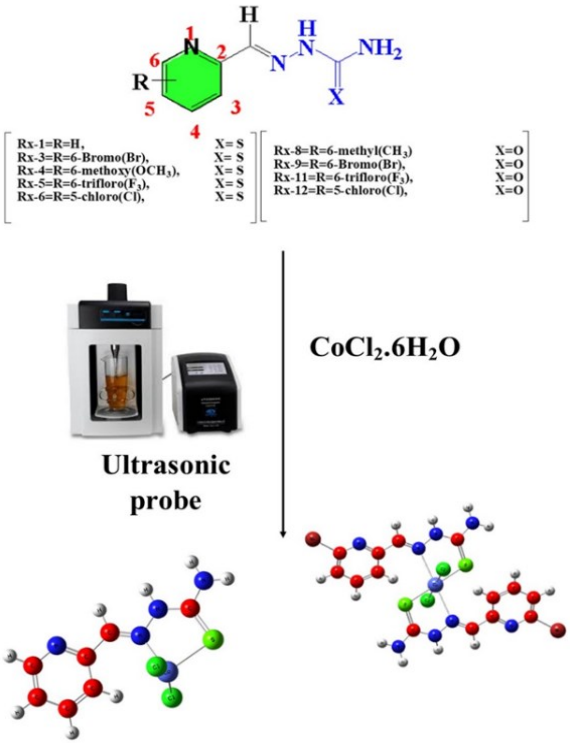

Scheme 1. Synthesis of cobalt complexes of pyridine carboxamide and carbothioamide.

Shape and surface topography

The surface topography and shape of the cobalt complexes of pyridine carboxaldehyde semicarbazone and thiosemicarbazone were characterized using an atomic force microscope (AFM). The study revealed the presence of polydisperse particles ranging in size from 11 to 60 nm. Upon inserting metal into the pyridine carboxaldehyde semicarbazone and thiosemicarbazone complexes, surfaces were transformed into uniformly sized smooth shapes, as depicted in the figures presented in the supplementary data. Specifically, complexes such as CoRx-1Cl_2, CoRx-3Cl_2, CoRx-4Cl_2, CoRx-5Cl_2, CoRx-6Cl_2, CoRx-8Cl_2, CoRx-9Cl_2, and CoRx-11Cl_2 exhibited surfaces that were more uniform in small needle-like structures, while the CoRx-12Cl_2 complex displayed a smooth, ball-like structure.

Cholinesterase inhibition potential

The newly synthesized cobalt complexes of pyridine carboxaldehyde semicarbazone and thiosemicarbazone underwent screening for cholinesterase inhibition potential, specifically targeting AChE and BuChE. The summarized results are presented in Table 1. Compounds demonstrating more than 50% inhibition were further assessed for their IC_{50} values. The findings indicated that all synthesized compounds selectively inhibited AChE, with IC_{50} values ranging from submicromolar to micromolar concentrations (0.97±0.02 µM to 6.47±0.71 µM), except for CoRx-1Cl_2, which exhibited inhibition of both AChE and BuChE, with IC_{50} values of 1.91±0.08 µM and 12.97±2.46 µM, respectively.

In this study, donepezil was utilized as a positive control, showing inhibition with IC_{50} values of 0.03±0.01 µM and 6.41± 0.34 µM for AChE and BuChE, respectively. The IC_{50} values of the synthetic inhibitors and the standard (donepezil) for AChE were ranked as follows: CoRx-8Cl_2 > CoRx-12Cl_2 > CoRx-5Cl_2 > CoRx-1Cl_2 > CoRx-3Cl_2 > CoRx-11Cl_2 > CoRx-4Cl_2 > CoRx-6Cl_2 > donepezil. Inhibiting the enzyme leads to acetylcholine accumulation, overstimulation of nicotinic and muscarinic receptors, and disruption of neurotransmission, which may improve the symptoms of Alzheimer's disease patients by restoring synaptic levels of this neurotransmitter.

- *Structure-activity relationship*

Among the tested compounds, only CoRx-1Cl_2 exhibited significant inhibition of both AChE and BuChE, with IC_{50} values of 1.91±0.08 µM and 12.97±2.46 µM, respectively. This could be attributed to the presence of a non-substituted pyridine ring in the structure.

CoRx-6Cl_2 demonstrated the most potent and selective inhibition of AChE, with an IC_{50} value of 0.97±0.02 µM. The presence of a chlorine (Cl) group substitution on the 5th position of the pyridine ring may contribute to this enhanced potency by reducing the electron density from the aromatic ring. This substitution strategy appears to be more effective compared to compounds with no substitution or substitution at the C-6 position of the pyridine ring.

Table 1. Cholinesterase inhibition assay results of cobalt complexes of pyridine carboxaldehyde

Sr. no	Compound name	Structure	AChE	BuChE
			$IC_{50} \pm$ SEM (μM) or (% inhibition ± SD)*	
1.	$CoRx\text{-}1Cl_2$	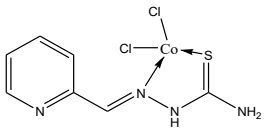	1.91±0.08	12.97±2.46
2.	$CoRx\text{-}3Cl_2$	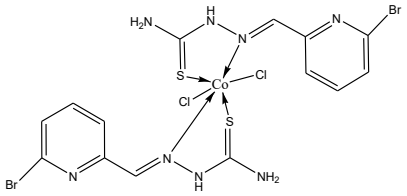	1.42±0.10	14%
3.	$CoRx\text{-}4Cl_2$	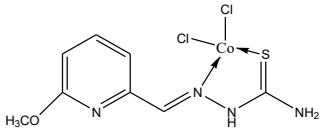	1.23±0.47	19%
4.	$CoRx\text{-}5Cl_2$	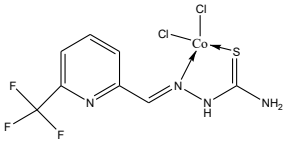	2.59±0.12	11%
5.	$CoRx\text{-}6Cl_2$	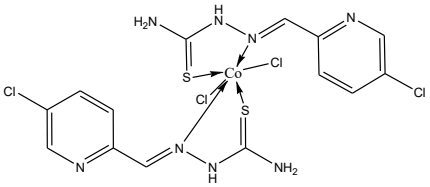	0.97±0.02	13%
6.	$CoRx\text{-}8Cl_2$	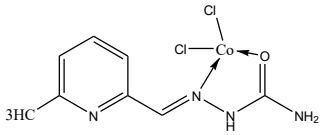	6.47±0.71	16%
7.	$CoRx\text{-}9Cl_2$	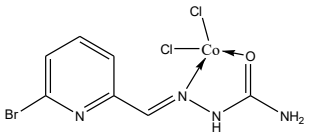	36%	14%
8.	$CoRx\text{-}11Cl_2$	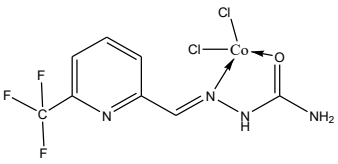	1.25±0.29	21%
9.	$CoRx\text{-}12Cl_2$	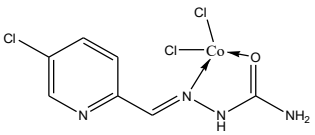	3.07±0.56	27%
10.	Donepezil		0.03±0.01	6.41± 0.34

Other compounds, including CoRx-4Cl_2 (IC_{50} = 1.23±0.47 µM), CoRx-11Cl_2 (IC_{50} = 1.25±0.29 µM), CoRx-3Cl_2 (IC_{50} = 1.42±0.10 µM), CoRx-5Cl_2 (IC_{50} = 2.59±0.12 µM), CoRx-12Cl_2 (IC_{50} = 3.07±0.56 µM), and CoRx-8Cl_2 (IC_{50} = 6.47±0.71 µM), also showed selective inhibition of AChE.

- *Docking study*

One of the most significant methods employed in structure-based drug design is molecular docking, which analyzes atomic-level interactions between a protein and a small molecule. In our study, we conducted docking analyses on the most potent cobalt complexes of pyridine carboxaldehyde thiosemicarbazone against AChE to establish a meaningful association between *in-vitro* and *in-silico* studies. The objective was to gain a deeper understanding of the essential relationships between active scaffolds and the enzyme's active sites.

During the analysis, active residues such as Tyr124 and Tyr337 exhibited hydrogen bonding with sulfur (S) and chlorine (Cl) atoms, while Trp286 showed hydrogen-arene interaction with the pyridine ring of CoRx-4Cl_2. Similarly, CoRx-6Cl_2 demonstrated binding interactions with Ser293 and Trp286, interacting with sulfur and chlorine atoms, while His287 exhibited hydrogen-arene interaction with the pyridine ring, as depicted in Figures 1 and 2.

According to literature, Tyr337 serves as an entrance point for the catalytic anionic binding site (CAS) for acetylcholine binding, while Trp286 is a principal component of the peripheral anionic site (PAS) that regulates the accessibility of small molecules to the active site and contributes to allosterism. Arene interactions with the Trp286 residue modulate inhibition constants for some AChE inhibitors [34-35]. CoRx-6Cl_2 exclusively demonstrated binding interactions at PAS, whereas CoRx-4Cl_2 exhibited binding interactions at both CAS and PAS by interacting with Tyr337 and Trp286, thereby enhancing its potency and selectivity.

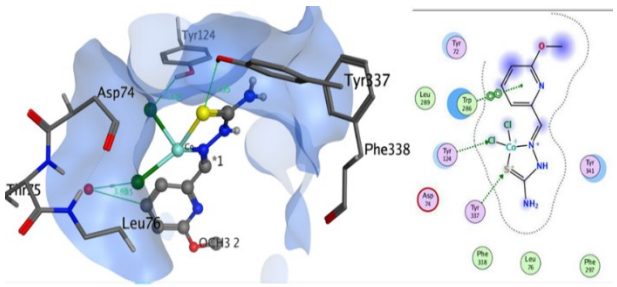

Figure 1. Docked image of CoRx-4Cl_2 at the active pocket site of AChE.

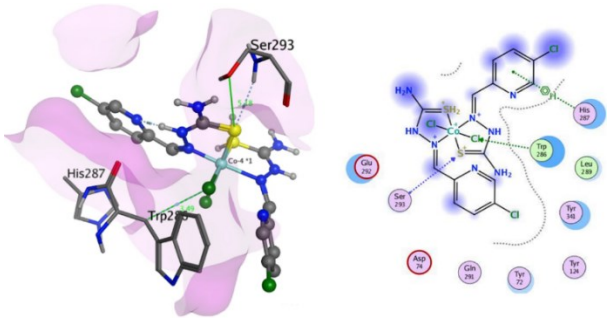

Figure 2. Docked image of CoRx-6Cl_2 at the active pocket site of AChE.

- *Kinetic study*

The Lineweaver-Burk plot of CoRx-6Cl_2 was generated to assess the competitive mode of inhibition between the tested molecule and the standard substrate, as illustrated in Figure 3. Kinetic studies revealed that as the concentration increases, Km also increases, with only minor differences observed, while Vmax remains constant without significant changes in slopes. This suggests that the substrate and inhibitor compete to bind at the active pocket.

The identified inhibitors demonstrated strong binding at the active pocket of AChE, a finding further validated through molecular docking studies [36].

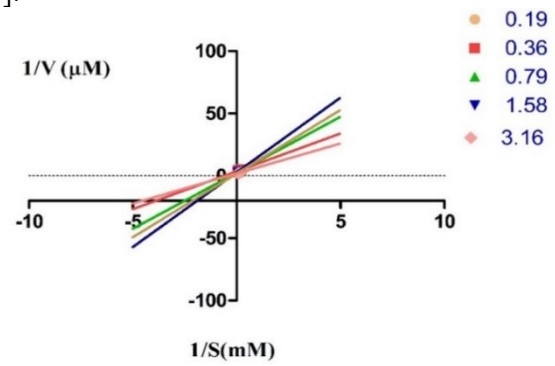

Figure 3. Lineweaver-Burk plot of CoRx-6Cl_2.

Anti-proliferative potential

The MTT assay was utilized to assess the anti-proliferative activity of cobalt complexes of pyridine carboxaldehyde semicarbazone and thiosemi-carbazone using the glioblastoma cell line (U87), while the cytotoxic activity was evaluated on the normal cell line HEK-293, as presented in Table 2. This cell line was chosen due to the compounds' potential efficacy against many enzymes associated with neurodegenerative diseases, suggesting they might also exhibit anti-proliferative potential.

Table 2. MTT assay result of cobalt complexes of pyridine carboxaldehyde semicarbazone and thiosemicarbazone.

Sr. no	Compound name	Structure	% Cell viability	
			HEK-293	U87
1.	CoRx-1Cl_2	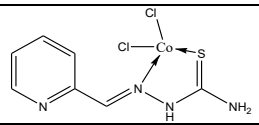	215.05	52.1
2.	CoRx-3Cl_2	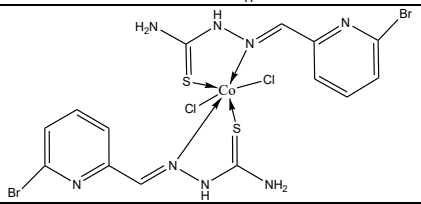	303.32	92.9
3.	CoRx-4Cl_2	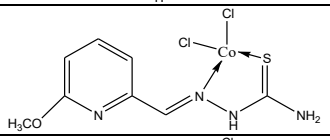	212.3	87.9
4.	CoRx-5Cl_2	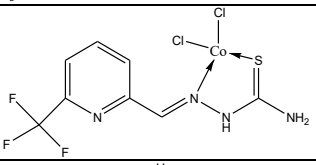	129.52	20.93
5.	CoRx-6Cl_2	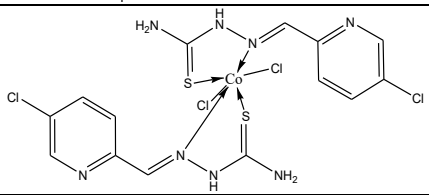	136.34	23.46
6.	CoRx-8Cl_2	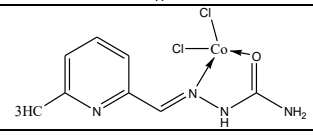	217.58	62.27
7.	CoRx-9Cl_2	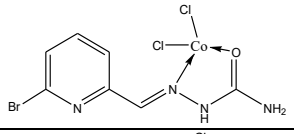	246.08	384.84
8.	CoRx-11Cl_2	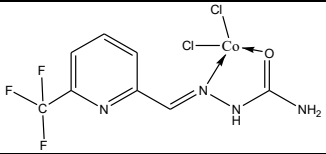	313.26	81.36
9.	CoRx-12Cl_2	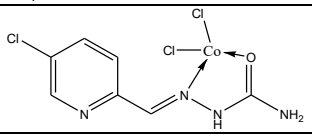	185.03	82.47
10.	Doxorubicin		82.2594	59.8512

The study revealed that all synthesized compounds were non-toxic to the normal cell line, as evidenced by cell viability increasing above 100% after 48 hours of incubation. This suggests that the tested molecules did not affect the growth of the normal cell line. In fact, upon incubation, the number of normal cell line cells doubled compared to the initially incubated cells. Conversely, in the case of U-87 cells, viability decreased from 100%. Among them, CoRx-5-Cl_2 and CoRx-6-Cl_2 showed the most potent results, indicating moderate to low anti-proliferative activity.

Metal complexes exhibited a stronger potential anti-proliferative effect due to the positive charge of the metal ions enhancing the acidity of the coordinated ligand. This facilitated the ligands carrying hydrogen ions to form stronger hydrogen bonds with the negatively charged DNA of cancer cells.

- *Structure-activity relationship*

The structure-activity relationship analysis revealed that the parent cobalt complex of pyridine carboxaldehyde thiosemicarbazone exhibited moderate anti-proliferative activity, with a cell viability of 52.1%. Substitution of bromo and methoxy groups at the 6th position of the pyridine ring of thiosemicarbazone led to a decrease in proliferative action, with cell viabilities of 92.9% and 87.9%, respectively. Conversely, substitution of trifluoro group at the 6th position and chloro group at the 5th position of the pyridine ring of thiosemicarbazone remarkably increased proliferative activity, with cell viabilities of 20.93% and 23.46%, respectively, even surpassing the standard drug doxorubicin, which showed 59.85% cell viability.

MATERIALS AND METHODOLOGY

The starting materials were purchased from Sigma-Aldrich and utilized directly without additional purification. Synthesis of the cobalt complexes was carried out using an ultrasonic probe, and their characterization was conducted using AFM, FTIR, and 1H-NMR spectroscopy.

Synthesis of cobalt complexes of pyridine carboxaldehyde semicarbazone and thiosemicarbazone

The precursor ligand solution was prepared by dissolving the pyridine semicarbazone and thiosemicarbazone [30] in an ethanol/water solution. Due to their low water solubility, they were initially dissolved in a small volume of ethanol and then the solution was made up with water to achieve a concentration of 0.001 molar. This solution was then added dropwise into a solution of cobalt chloride hexahydrate ($CoCl_2.6H_2O$) of the same concentration. The mixture was placed in a high-density ultrasonic probe with an operating frequency of 37 kHz and a force output of 320 W. After sonication for a full half hour, the products were precipitated out, filtered, washed with ethanol, allowed to air-dry, and finally stored in a closed container.

*CoRx-1*Cl_2 *(*$C_7H_8Cl_2CoN_4S$*)* Molecular weight = 310 g/mol; yellow color; yield = 74%; melting point= 270°C, FTIR (KBr, cm^{-1}): 837 (C=S), 1581 (C=N), 3390 (NH); Elemental analysis (calculated): C = 27.03, H = 2.92, N =18.01, S= 10.31, Co= 18.94, Cl = 22.79; ^{1}H-NMR 500 MHz, DMSO-d_6; δ_H = 7.369 (t, 1H), 7.821 (t, 1H), 8.082 (s, 1H), 8.180 (s, 1H), 8.272-8.286 (d, 1H), 8.557 (d,1H), 11.642 (s, 1H).

*CoRx-3*Cl_2 *(*$C_{14}H_{14}Br_2Cl_2CoN_8S_2$*)* Molecular weight = 650 g/mol ;brown color; yield = 63%; Melting point = 255°C; FTIR (KBr, cm^{-1}): 793 (C=S), 1451 (C=N), 3344 (NH); Elemental analysis (calculated): C = 25.86, H = 2.48, Br = 24.58, N= 17.24, S= 9.86, Co= 9.07, Cl=10.91; ^{1}H- NMR 500 MHz, DMSO-d_6; δ_H = 7.6150-7.6279 (d,2H), 7.767-7.792 (t,2H), 7.976 (s,1H), 8.263 (s,2H), 8.325-8.338(d,2H), 11.741 (s,1H).

*CoRx-4*Cl_2 *(*$C_8H_{11}Cl_2CoN_4OS$*)* Molecular weight = 341 g/mol; peach color; Yield = 54%; Melting point = 280°C, FTIR (KBr, cm^{-1}): 799 (C=S), 1612 (C=N), 3371 (NH); Elemental analysis (calculated): C =28.17, H= 3.25, N= 16.43, O= 4.69, S= 9.40, Co= 17.28, Cl= 20.79; ^{1}H- NMR 500 MHz, DMSO-d_6; δ_H 4.009 (s,3H), 7.012-7.025 (d, 1H), 7.357-7.376 (d,1H), 7.944-7.971(t,1H), 8.2032 (s,1H), 8.587 (s,1H), 13.84 (s,1H).

*CoRx-5*Cl_2 *(*$C_8H_8Cl_2CoF_3N_4S$*)* Molecular weight = 379 g/mol; light pink; Yield = 60%; melting point = 263°C, FTIR (KBr, cm^{-1}): 818 (C=S), 1595 (C=N), 3426 (NH), Elemental analysis (calculated): C = 25.35, H = 2.13, F= 15.04, N= 14.78, S= 8.46, Co = 15.55, Cl = 18.70; ^{1}H-NMR 500 MHz, DMSO-d_6 ; δ_H = 7.868-7.881 (d,1H), 8.084-8.130 (q,2H), 8.348 (s,1H), 8.488 (s,1H), 11.817 (s, 1H).

*CoRx-6*Cl_2 *(*$C_{14}H_{16}Cl_4CoN_8S_2$*)* Molecular weight = 561 g/mol; brown color; Yield = 82%; melting point = 230°C, FTIR (KBr, cm^{-1}): 828 (C=S), 1444 (C=N); Elemental analysis (calculated): C= 29.96, H= 2.87, N= 19.97, S= 11.43, Co= 10.50, Cl= 25.27; ^{1}H-NMR 500 MHz, DMSO-d_6; δ_H = 7.980 (d, 2H), 8.068 (s,2H), 8.272 (s, 2H), 8.350-8.397 (d, 2H), 8.610 (s, 2H), 11.693 (s, 1H).

*CoRx-8*Cl_2 *(*$C_8H_{10}Cl_2CoN_4O$*)* Molecular weight = 308 g/mol; dirty white; Yield = 73%; melting point = 310°C, FTIR (KBr, cm^{-1}): 1542 (C=N), 1662 (C=O); Elemental analysis (calculated): C= 31.19, H =3.27, N= 18.19, O= 5.19, Co=19.13, Cl= 23.02; ^{1}H-NMR 500 MHz, DMSO-d_6; δ_H= 2.452 (s, 3H), 6.596 (s,1H), 7.173-7.186 (d,1H), 7.661-7.687 (t,1H), 7.825(s,1H),7.934- 7.947 (d,1H), 10.475 (s,1H).

*CoRx-9*Cl_2 *(*$C_7H_7BrCl_2CoN_4O$*)* Molecular weight = 372 g/mol; light pink; Yield= 64%; melting point= 240°C, FTIR (KBr, cm^{-1}): 1540 (C=N), 1695 (C=O); Elemental analysis (calculated): C= 22.55, H= 1.89, Br= 21.43, N= 15.02, O= 4.29,Co=15.80, Cl=19.01; ^{1}H-NMR 500 MHz, DMSO-d_6; δ_H = 6.705 (s,1H), 7.572 (d,1H), 7.752-7.778 (q, 2H), 8.202 (s, 1H), 10.641 (s,1H).

*CoRx-11*Cl_2 *(*$C_8H_7Cl_2CoF_3N_4O$*)* Molecular weight = 360 g/mol; peach color; Yield = 69%; melting point = 240°C, FTIR (KBr, cm^{-1}): 1584 (C=N), 1714 (C=O); Elemental analysis

(calculated): C= 26.54, H= 1.95, F= 15.74, N= 15.48, O= 4.42, Co=16.28, Cl= 19.59,; ^{1}H-NMR 500 MHz, DMSO-d_6; δ_H = 6.771 (s,1H),7.82 (d,1H), 7.90 (s,1H), 8.09(t,1H), 8,497 (d,1H), 10.726 (s,1H).

CoRx-12Cl$_2$ ($C_7H_7Cl_3CoN_4O$) Molecular weight = 328 g/mol; off white; Yield = 71%, melting point= 320°C, FTIR (KBr, cm^{-1}): 1586 (C=N), 1698 (C=O); Elemental analysis (calculated): C= 25.60, H= 2.15, N= 17.06, O= 4.87, Co= 17.94, Cl= 32.38; ^{1}H-NMR 500 MHz, DMSO-d_6; δ_H = 6.690 (s,1H), 7.860 (s, 1H), 7.941 (d, 1H), 8.224 (d,1H), 8.573 (s, 1H), 10.570 (s,1H).

Cholinesterase inhibition assay

Ellman's method [37] was employed to assess the inhibitory potential of AChE (acetylcholinesterase) with EC Number: 3.1.1.7 and BuChE (butyryl-cholinesterase) with EC Number: 3.1.1.8, with minor modifications. For the assay, 10 µL of the test molecule (1 mM, 10% DMSO), 50 mM phosphate buffer (KH_2PO_4) at pH 7.8, and 10 µL of the enzymes (0.029 and 0.5 U/mL of AChE or BuChE, respectively) were combined and incubated for 10 minutes at 37°C. Following this, 10 µL of 1 mM acetylthiocholine iodide or butyrylthiocholine chloride and 10 µL of 5,5-dithiobis-2-nitrobenzoic acid reagent (5 mM) were added to each individual enzyme solution. Enzymatic reactions were measured using a microplate reader (FLUOstar Omega, BMG Labtech, Germany) at 405 nm following a 30-minute incubation period at 37°C. The IC_{50} values of compounds showing more than 50% inhibition in three replicates were calculated by further diluting the compound into eight different concentrations.

- *Docking study*

The most potent inhibitors among the tested compounds underwent molecular docking investigations using Molecular Operating Environment software (MOE version 2019, Chemical Computing Group, Montreal, QC, Canada). Prior to docking, the Chem 3D v20.0 software was utilized to minimize the energy of the drawn structure. The Force-Field-based parameterization and energy minimization was done by using the MMFF94x force field. Crystal structures of AChE (PDB ID; 4EY4) and BuChE (PDB ID; 1P0I) were downloaded from the RSCB database (https://www.rcsb.org/).

The default parameters (T: 300, pH:7, Salt: 0.1, Dielectric: 2, Cutoff(A) 15, solvent: 89 van der Waals; 800r3, Electrostatic; GB/VI) for docking in the MOE software were applied to the crystal structures. Active amino acid residues were selected using the site finder tool for active site identification after removal of the standard ligand and co-factor from the active pocket. Rapid preparation of the crystal structure was then completed. Docking was performed with default parameters, and the top 20 poses were selected for further analysis.

- *Kinetic study*

To elucidate the mechanism of inhibition for AChE and BuChE, the most potent inhibitor was utilized in enzyme kinetic investigations. The experiment involved testing various concentrations of the test chemicals (0.19 µM, 0.36 µM, 0.79 µM, 1.58 µM, 3.16 µM in DMSO), along with different amounts of the substrate, namely Donepezil (0 mM, 5 mM, 10 mM, 15 mM, and 20 mM).

Anti-proliferative activity

The synthetic compounds' antiproliferative activity was assessed using HEK-293 and U-87 cells, with doxorubicin serving as a positive control. These cells were seeded in 96-well plates at a density of approximately 10,000 cells per well and incubated for 24 hours to achieve a uniform single layer of cells. Subsequently, the cell lines were treated in triplicate with the tested drugs at various doses (i.e., 1, 2.5, 5, 10, 15, 20, and 25 µM in DMSO) and incubated under a flow of carbon dioxide for 48 hours at 37°C.

Following the incubation period, the cells were treated with 30 µL of MTT solution (5 mg/ml) and incubated for additional 4 hours at 37°C. The absorbance of the MTT formazan formed was quantified using an ELISA plate reader set to 540 nm.

$$\%\ Cell\ viability = \frac{(\text{A sample} - \text{A blank})}{(\text{A control} - \text{A blank})} \times 100$$

CONCLUSION

In conclusion, given the absence of a cure for Alzheimer's disease (AD), cholinesterase inhibitors like Donepezil have been employed to delay its progression. Currently, second-generation cholin-esterase inhibitors such as rivastigmine and galantamine are utilized in AD treatment. The objective of this research is to identify novel inhibitors to further advance AD treatment by leveraging the intriguing properties of transition metal complexes. To assess their potential as multi-targeting medications, acetylcholinesterase (AChE), butyrylcholinesterase (BuChE), and proliferative *in-vitro* assays were employed to evaluate each compound. Analysis of the structure–activity relationships revealed that variations in activities were attributable to the various substituent patterns at different positions on the pyridine ring. Among the compounds tested, CoRx-6Cl$_2$ was identified as

the most potent AChE inhibitor and also demonstrated moderate anti-proliferative activity by inhibiting the U-87 cell line. This suggests its potential as a promising candidate for further investigation as a therapeutic agent for AD and potentially other related conditions.

***Conflict of interest*:** *Authors declare no conflict of interest.*

Acknowledgement: *Asia Naz Awan designed the study, Ayesha Naseer performed the synthesis and characterization study of the synthesized compounds, writeup the first draft of the manuscript, Sabahat Habib helped out to carry out proliferative assay, Jamsheed Iqbal and Aneela Javed reviewed the final manuscript.*

Supportive/supplementary material: *The AFM images, FTIR, ^{1}H-NMR, structures are presented in the supplementary file.*

REFERENCES

1. D. Small, Z. Ismael, I. J. N. Chubb, *Neuroscience*, **19**(1), 289 (1986).
2. K. J. M. Sharma, *Molecular Medicine Report*, **20**(2),1479 (2019).
3. L Jaganathan, R. J. B. Boopathy, *BMC Biochemistry*, **1**(1), 1 (2000).
4. J. A. Driver, A. Beiser, R. Au, B. E. Kreger, G. L. Splansky, T. Kurth, D. P. Kiel, K. P. Lu, S. Seshadri, P. A. J. B. Wolf, *BMJ*, **344**, (2012).
5. F. Catalá-López, B. Crespo-Facorro, E. Vieta, J. M. Valderas, A. Valencia, R. J. N. Tabarés-Seisdedos, *Neuroepidemiology*, **42**(2), 121, (2014).
6. H. Hussain, S. Ahmad, S. W. A. Shah, M. Ghias, A. Ullah, S. U. Rahman, Z. Kamal, F. A. Khan, N. M. Khan, J. J. M. Muhammad, *Molecules*, **26**(23), 7168 (2021)..
7. H. Hussain, S. Ahmad, S. W. A. Shah, A. Ullah, N. Ali, M. Almehmadi, M. Ahmad, A. A. K. Khalil, S. B. Jamal, H.J.M. Ahmad, *Molecules*, **27**(8), 2468 (2022). .
8. K. Popat, K. McQueen, T. W. Feeley, *Best Practice & Research Clinical Anaesthesiology*, **27**(4), 399 (2013)..
9. J. B. J. S. Gibbs, *Science*, **287**(5460), 1969 (2000).
10. H. J. S. Varmus, *Science*, **312**(5777), 1162 (2006).
11. M. Khudhayer Oglah, Y. J. M. C. R. Fakri Mustafa, *Medicinal Chemistry Research*, **29**(3), 479, (2020).
12. H. J. Xi, R. P. Wu, J. J. Liu, L .J. Zhang, Z. S. J. T. C. Li, *Thoracic Cancer*, **6**(4), 390 (2015).
13. O. I. Okereke, M. E. Jno Meadows, *Jama Network Open*, **2**(6), e196167 (2019).
14. J. Jończyk, J. Godyń, E. Stawarska, B. Morak-Młodawska, M. Jeleń, K. Pluta, B. J. M. Malawska, *Molecules*, **25**(11), 2604 (2020).
15. A. Daina, O. Michielin, V. J. S. Zoete, *Scientific Reports*, **7**(1), 1 (2017).
16. G. G. Mohamed, B. *Spectrochim. Acta A: Molecular and Biomolecular Spectroscopy,* **64**(1), 188 (2006).
17. M. T. H. Tarafder, M. A. Ali, N. Saravanan, W. Y. Weng, S. Kumar, N. Umar-Tsafe, K. A. Crouse, *Transition Metal Chemistry*, **25**(3), 295 (2000). .
18. H. Wilfredo, P. J. J. C. S. Juan, *Journal of Chemical Science*, **14**, 10 (2006). .
19. T. R. Todorović, J. Vukašinović, G. Portalone, S. Suleiman, N. Gligorijević, S. Bjelogrlić, K. Jovanović, S. Radulović, K. Anđelković, A. J. M. Cassar, *MedChemComm*, **8**(1), 103 (2017)..
20. S. M. Dawoud, *Journal of Physics: Conference Series,* IOP Publishing, 022059 (2021).
21. H. Beraldo, D. J. M. Gambino, *Mini-Reviews in Medicinal Chemistry*, **4**(1), 31 (2004).
22. D. C. Quenelle, K. A. Keith, E.R. Kern, *Antiviral Research*, **71**(1), 24 (2006).
23. S. A. Andres, K. Bajaj, N. S. Vishnosky, M. A. Peterson, M. S. Mashuta, R. M. Buchanan, P. J. Bates, C. A. Grapperhaus, *Inorganic Chemistry*, **59**(7), 4924 (2020).
24. D. C. Reis, A. A. R. Despaigne, J. G. D. Silva, N. F. Silva, C. F. Vilela, I. C. Mendes, J. A. Takahashi, H. J. M. Beraldo, *Molecules*, **18**(10), 12645 (2013).
25. M. Mackenzie, D. Saltman, H. Hirte, J. Low, C. Johnson, G. Pond, M. J. Moore, *Investigational New Drugs*, **25**(6), 553 (2007).
26. A. A. Aly, E. M. Abdallah, S. A. Ahmed, M. M. Rabee, E.-S. Abdelhafez, *Journal of Molecular Structure*, 133480, (2022).
27. B. M. Zeglis, V. Divilov, J. S. Lewis, *Journal of Medicinal Chemistry*, **54**(7), 2391 (2011). .
28. D. Osmaniye, B. Kurban, B. N. Sağlık, S. Levent, Y. Özkay, Z. A. Kaplancıklı, *Molecules*, **26**(21), 6640 (2021).
29. R. Jawaria, M. Hussain, H. B. Ahmad, M. Ashraf, S. Hussain, M. M. Naseer, M. Khalid, M. A. Hussain, M. Al-Rashida, M.N. Tahir, *Inorg. Chim. Acta*, **508**, 119658 (2020).
30. M. S. Ağırtaş, *Heterocyclic Communications*, **23**(1), 7 (2017).
31. I. Ali, Haque, A. Wani, W. A. Saleem, K. Al Za'abi, M., *Biomedical Chromatography*, **27**(10), 1296 (2013).
32. I. Ali, W. A. Wani, K. Saleem, M. F. Hsieh, *RSC Advances*, **4**(56), 29629 (2014).
33. A. Naseer, F. A. Osra, A. N. Awan, A. Imran, A. Hameed, S. A. Ali Shah, *et al*. *Pharmaceuticals*, **15**(10), 1288(2022).
34. J. L. Sussman, M. Harel, F. Frolow, C. Oefner, A. Goldman, L. Toker, I. Silman, *Science*, **253**(5022), 872 (1991).
35. A. Štalic, Z. Grubič, M. Šentjuric, S. Pečar, M. K. Gentry, B. P. Doctor, *Enzymes of the Cholinesterase Family*, **125** (1995).
36. N. A. Khan, I. Khan, S. Abid, S. Zaib, A. Ibrar, H. Andleeb, *et al., Medicinal Chemistry*, **14**(1), 74 (2018).
37. A. Komersova, K. Komers, A. Čegan, *Zeitschrift für Naturforschung C*, **62**(1-2), 150, (2007).

Supplementary data

CoRx-1-Cl$_2$

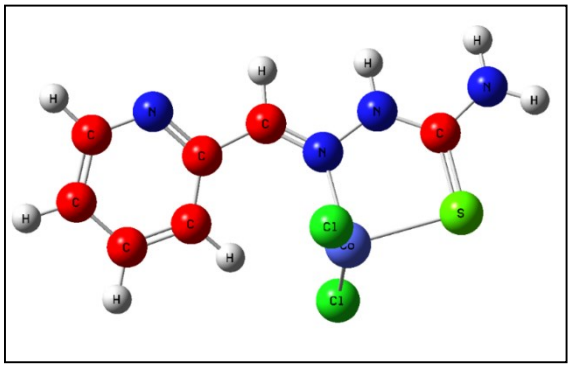

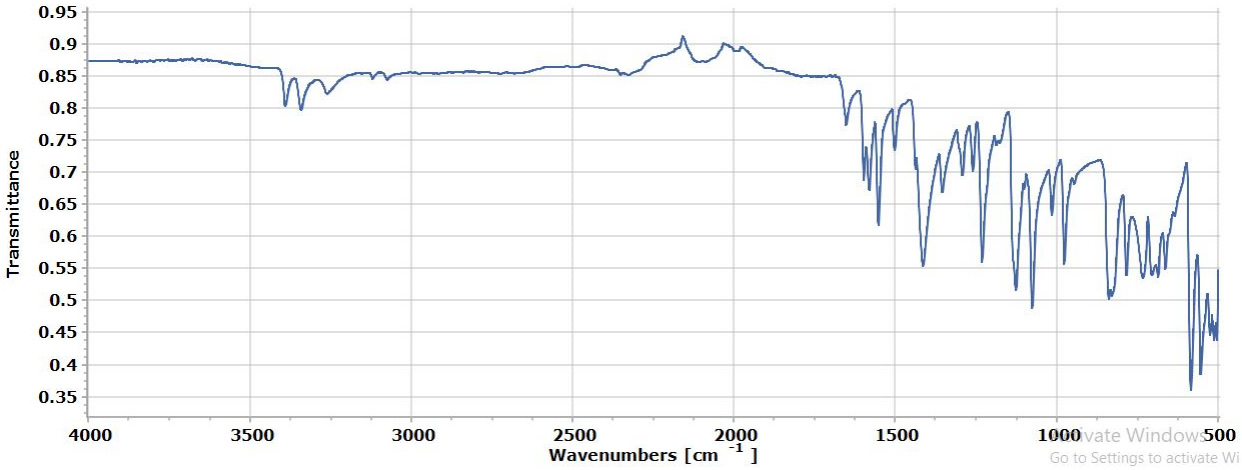

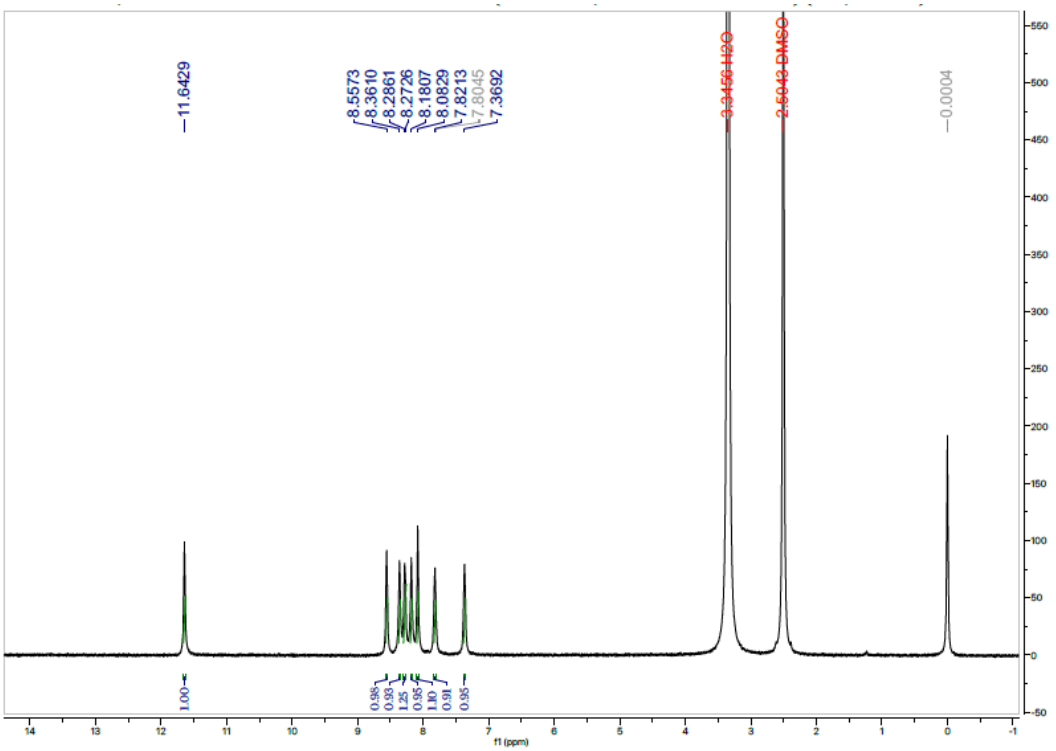

CoRx-3-Cl2

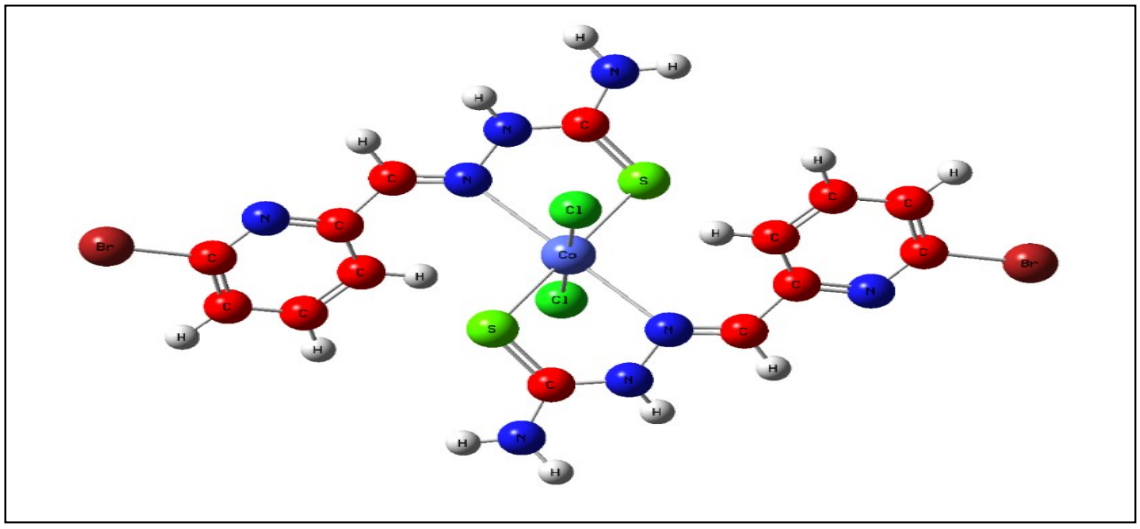
H
N
C
S
Cl
Co
Br

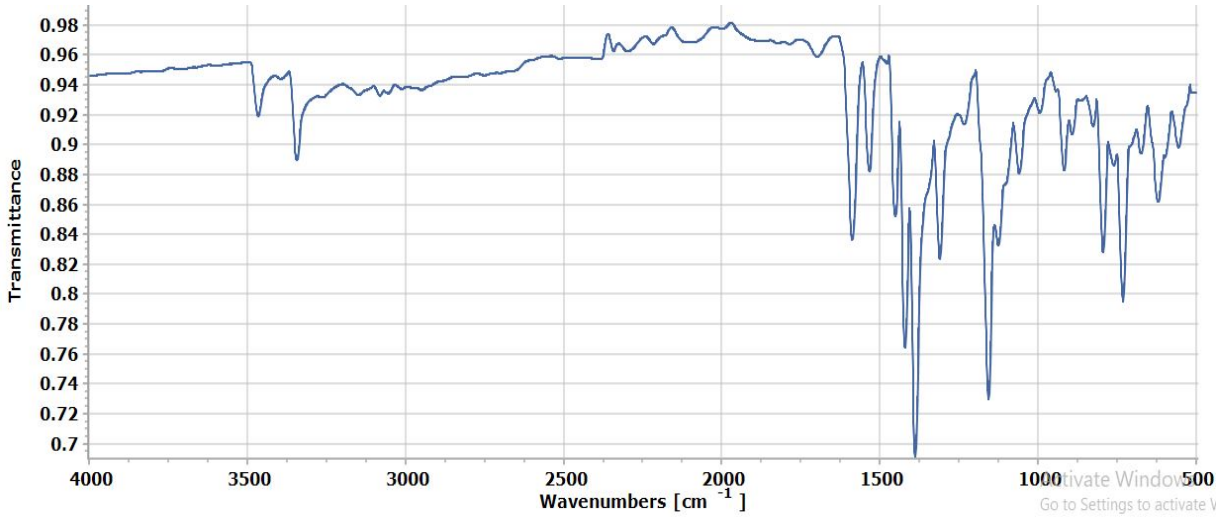
Transmittance
0.98
0.96
0.94
0.92
0.9
0.88
0.86
0.84
0.82
0.8
0.78
0.76
0.74
0.72
0.7
4000
3500
3000
2500
2000
1500
1000
500
Wavenumbers [cm -1]

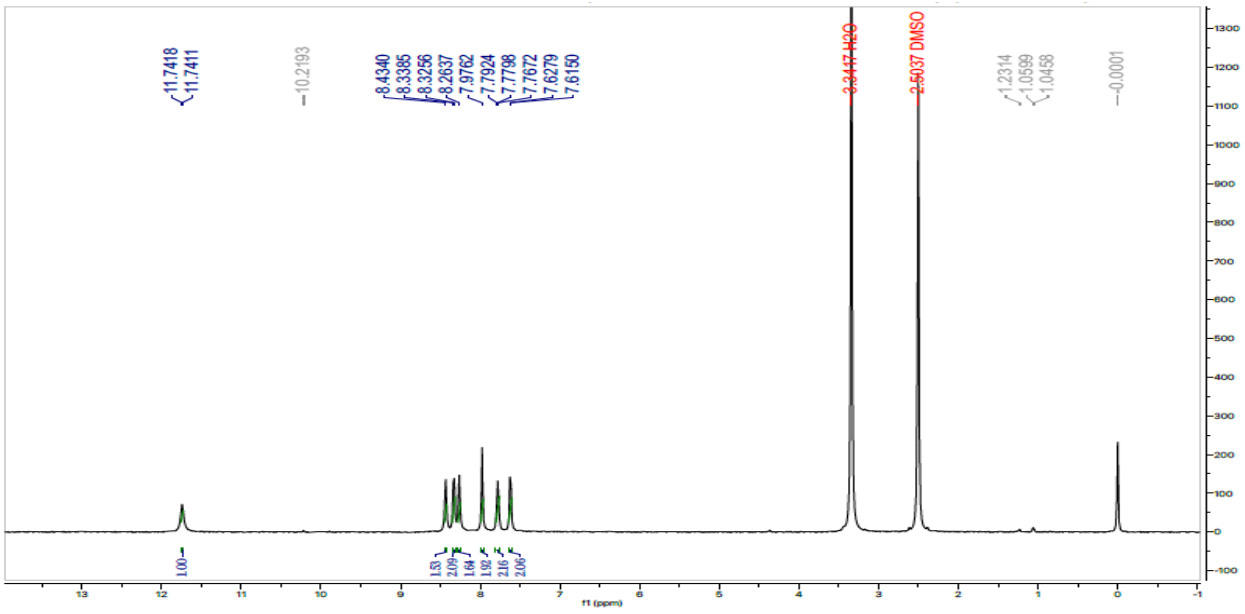
11.7418
11.7411
10.2193
8.4340
8.3385
8.3266
8.2637
7.9762
7.7924
7.7798
7.7672
7.6279
7.6150
3.3417 H2O
2.5037 DMSO
1.2314
1.0599
1.0488
0.0001
1.00
1.33
2.09
1.64
1.92
2.16
2.06
f1 (ppm)

CoRx-4-Cl$_2$

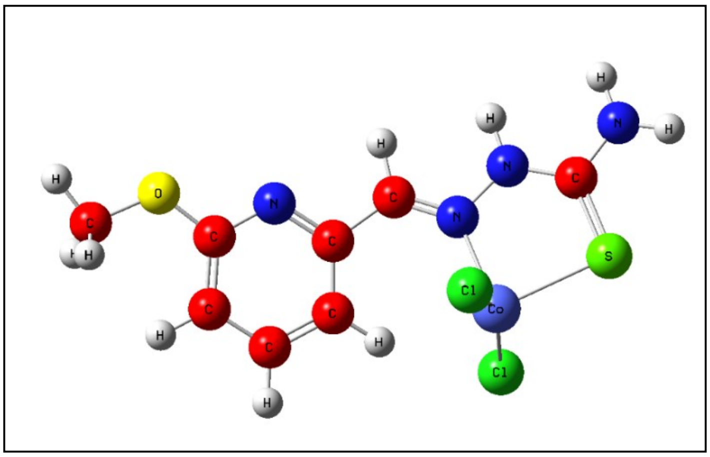
H
O
C
H
H
C
N
C
H
C
N
N
H
C
N
H
H
S
Cl
Co
Cl
C
C
C
H
H
H

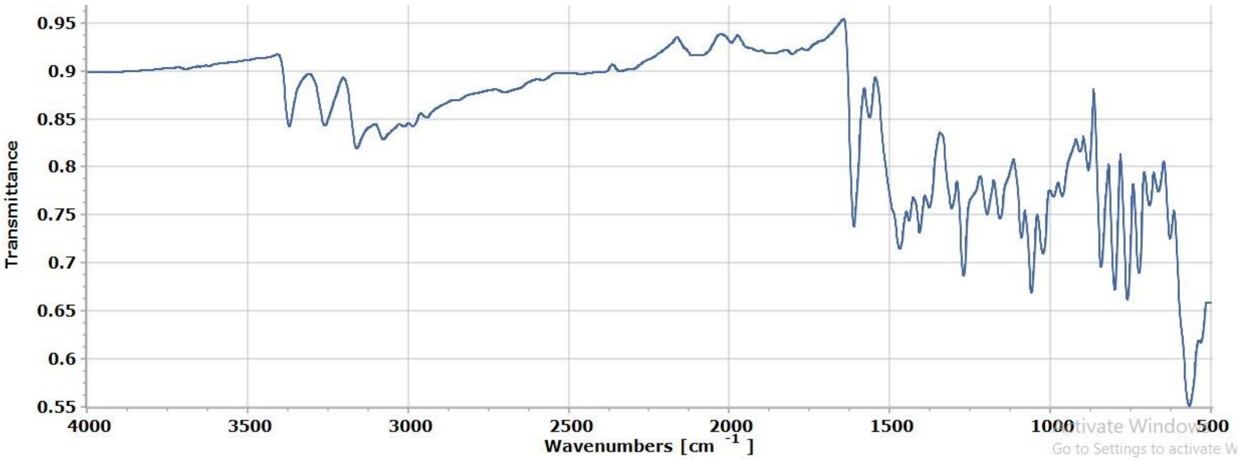
Transmittance
0.95
0.9
0.85
0.8
0.75
0.7
0.65
0.6
0.55
4000
3500
3000
2500
2000
1500
1000
500
Wavenumbers [cm^{-1}]

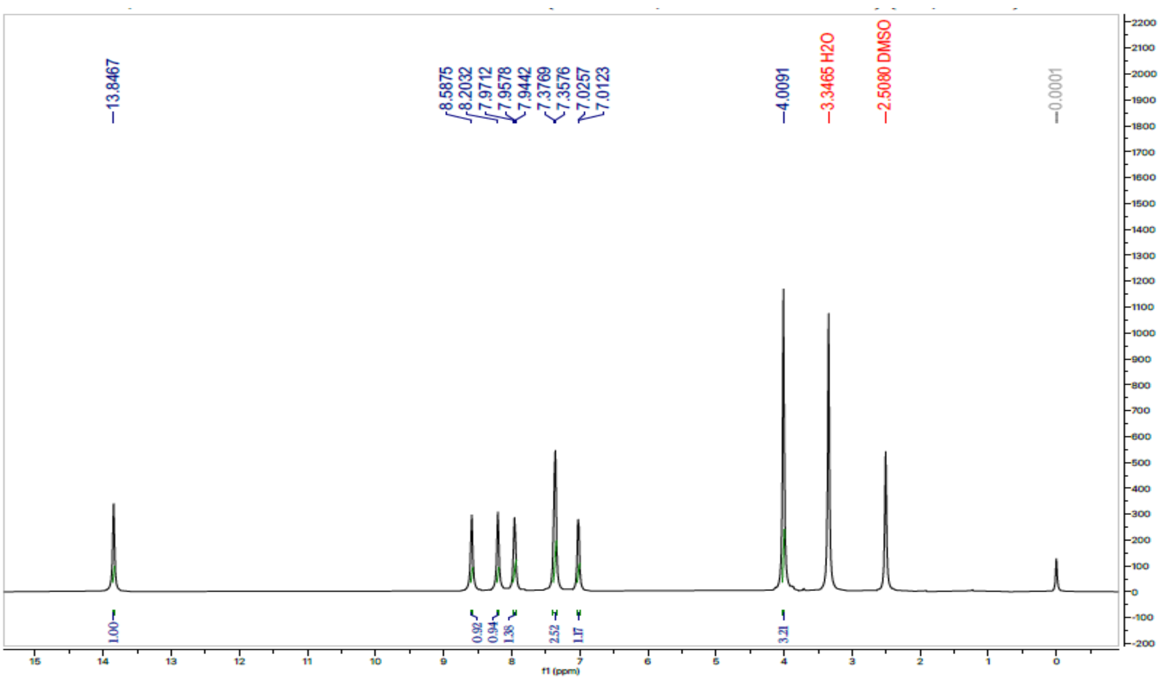
13.8467
8.5875
8.2032
7.9712
7.9578
7.9442
7.3769
7.3576
7.0257
7.0123
4.0091
3.3465 H2O
2.5080 DMSO
0.0001
1.00
0.92
0.94
1.38
2.52
1.17
3.21
f1 (ppm)

CoRx-5-Cl2

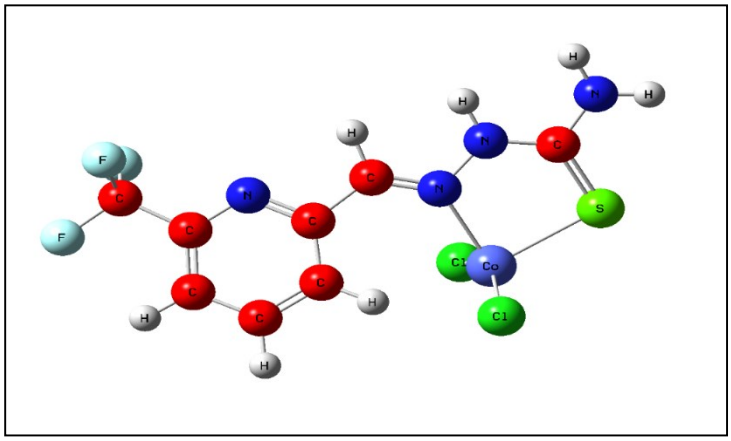
H
N
H
H
N
C
F
C
N
C
S
F
C
C
C1
Co
C
C
H
C
H
H

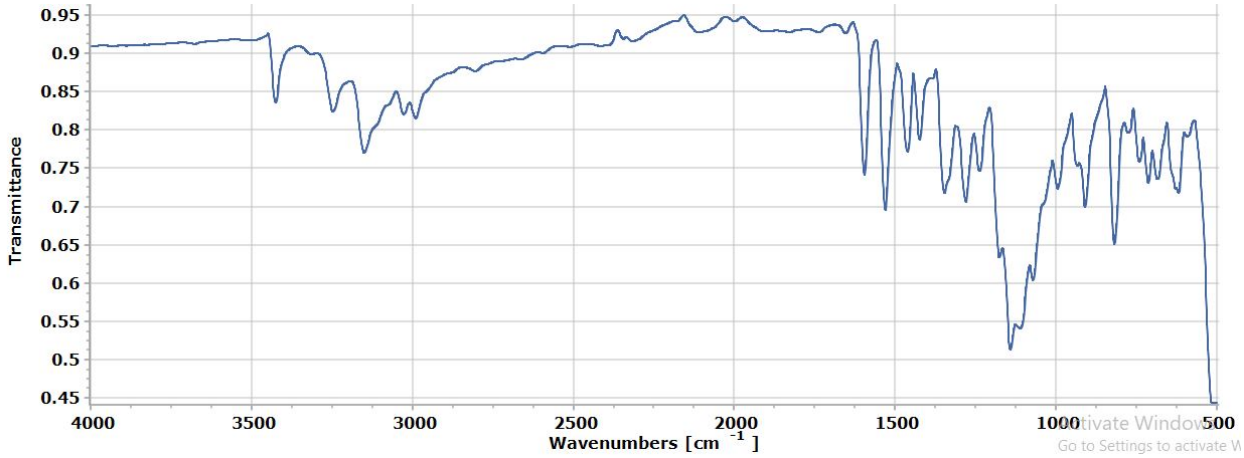
Transmittance
0.95
0.9
0.85
0.8
0.75
0.7
0.65
0.6
0.55
0.5
0.45
4000
3500
3000
2500
2000
1500
1000
500
Wavenumbers [cm -1]

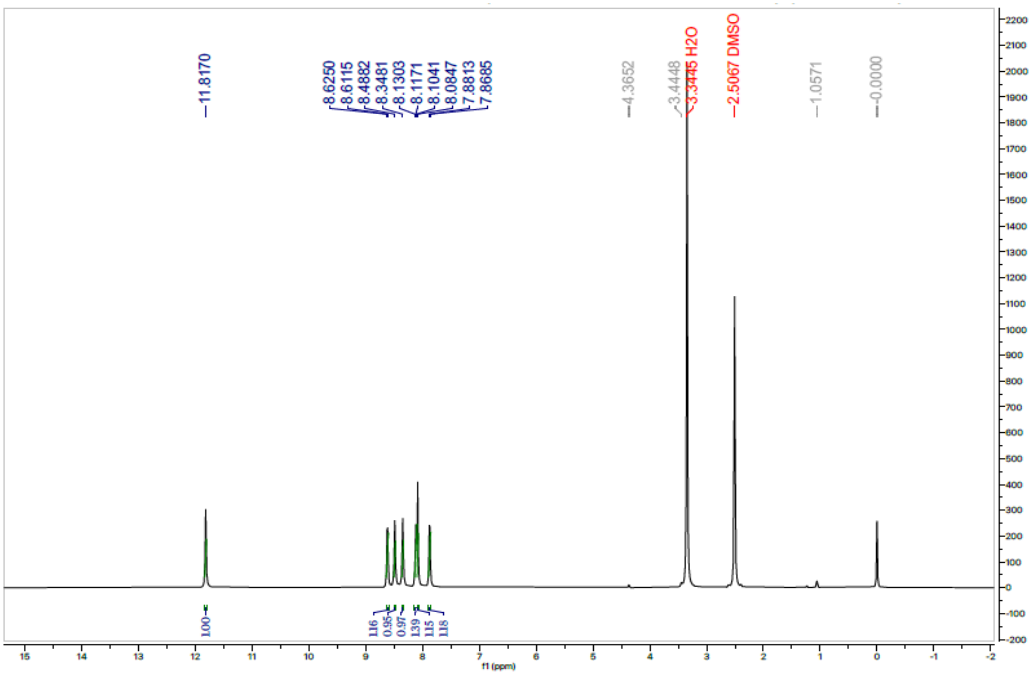
11.8170
8.6250
8.6115
8.4882
8.3481
8.1303
8.1171
8.1041
8.0847
7.8813
7.8685
4.3652
3.4448
3.3445 H2O
2.5067 DMSO
1.0571
0.0000
1.00
1.16
0.95
0.97
1.39
1.15
1.18
f1 (ppm)

CoRx-6-Cl2

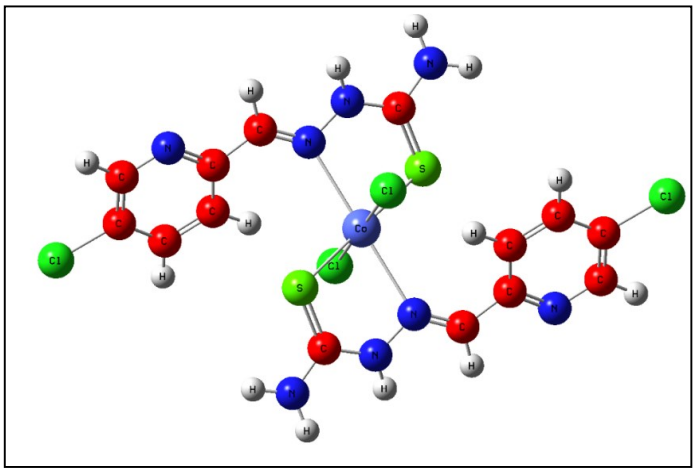

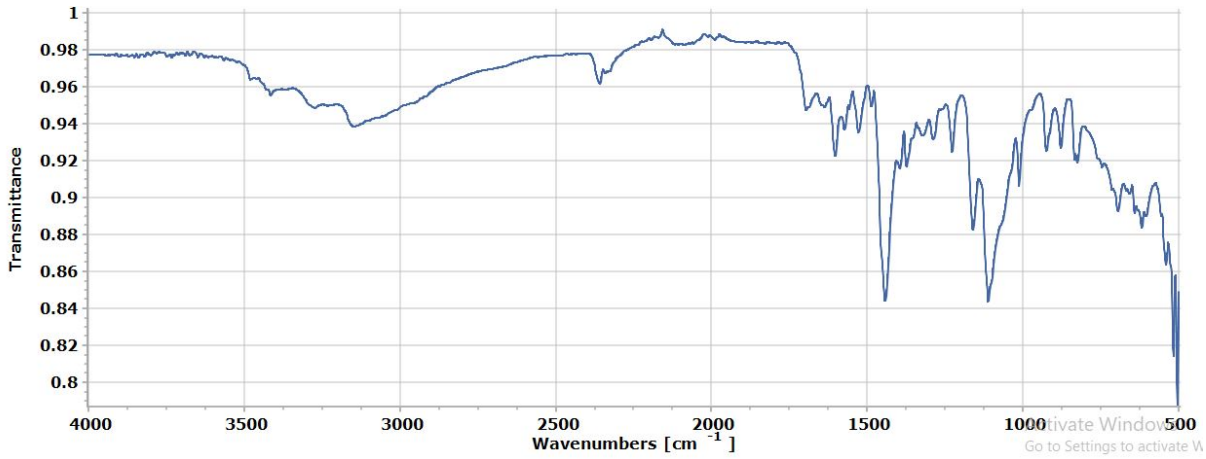
Transmittance
Wavenumbers [cm -1]
1
0.98
0.96
0.94
0.92
0.9
0.88
0.86
0.84
0.82
0.8
4000
3500
3000
2500
2000
1500
1000
500

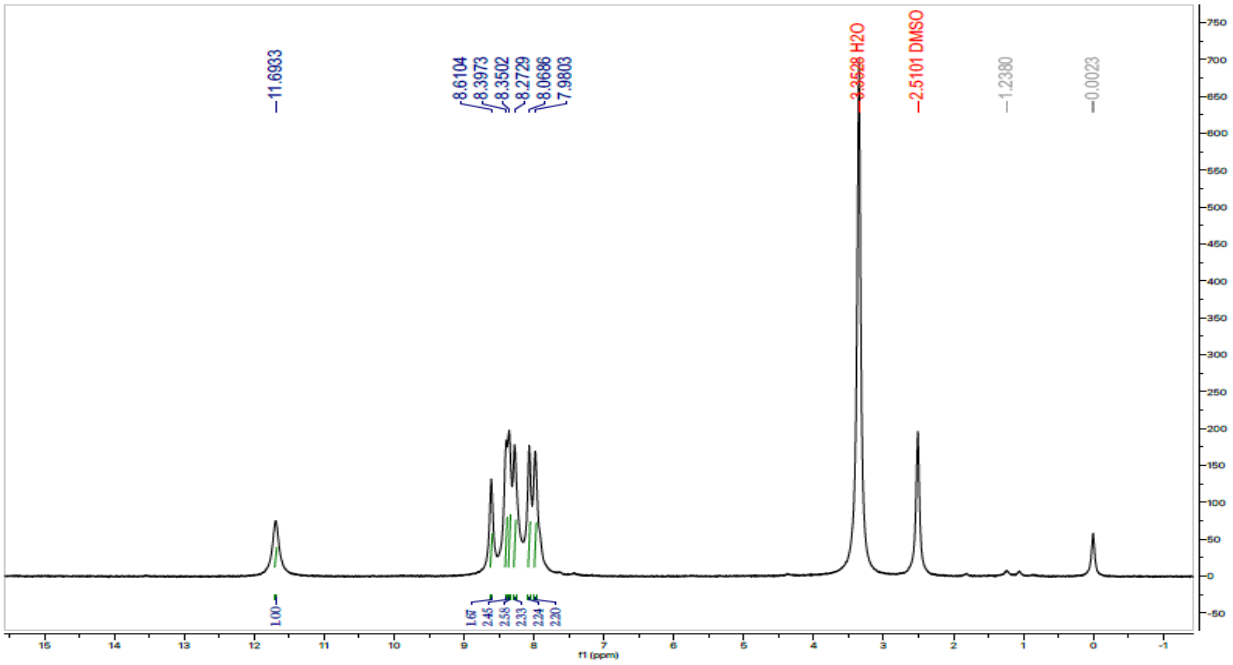
11.6933
8.6104
8.3973
8.3502
8.2729
8.0686
7.9803
3.3528 H2O
2.5101 DMSO
1.2380
0.0023
1.00
1.67
2.45
2.58
2.33
2.24
2.20
f1 (ppm)

CoRx-8-Cl$_2$

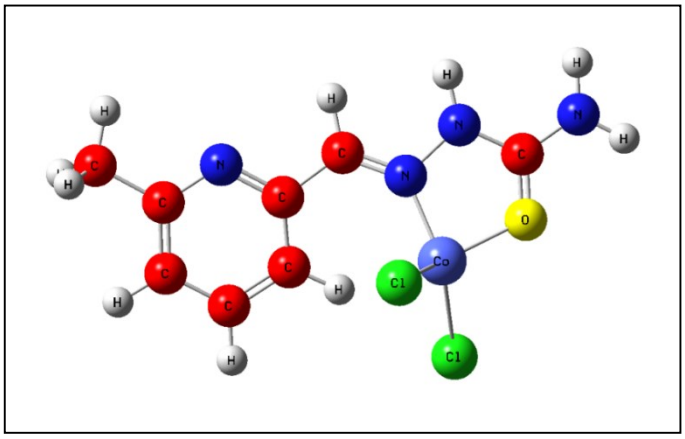
H
C
N
O
Co
Cl1
Cl1

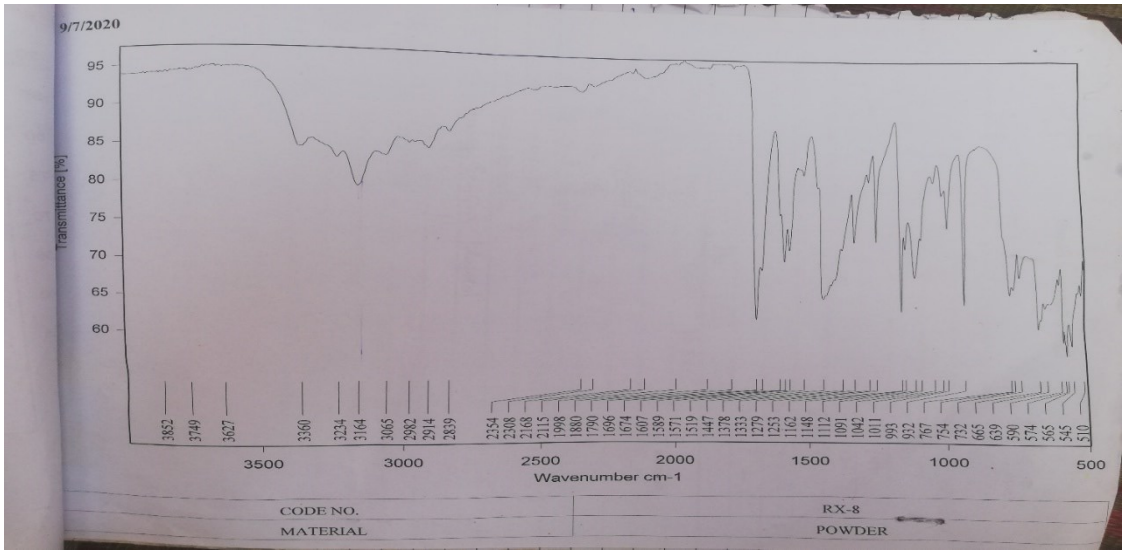
9/7/2020
Transmittance [%]
95
90
85
80
75
70
65
60
3852
3749
3627
3360
3224
3164
3065
2982
2914
2839
2354
2308
2168
2115
1998
1880
1790
1696
1674
1607
1589
1571
1519
1447
1378
1333
1279
1253
1162
1148
1112
1091
1042
1011
993
932
767
754
732
665
639
590
574
565
545
510
3500
3000
2500
2000
1500
1000
500
Wavenumber cm-1
CODE NO.
RX-8
MATERIAL
POWDER

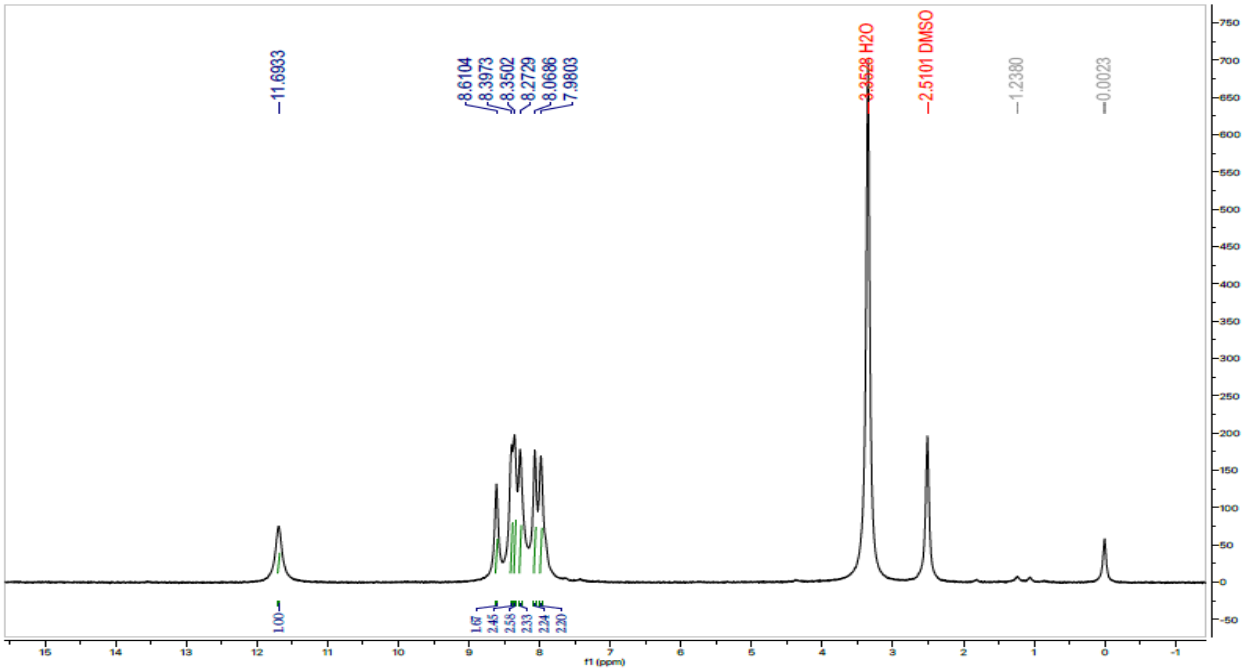
11.6933
8.6104
8.3973
8.3502
8.2729
8.0686
7.9803
3.3528 H2O
2.5101 DMSO
1.2380
0.0023
1.00
1.67
2.45
2.58
2.33
2.24
2.20
f1 (ppm)

CoRx-9-Cl$_2$

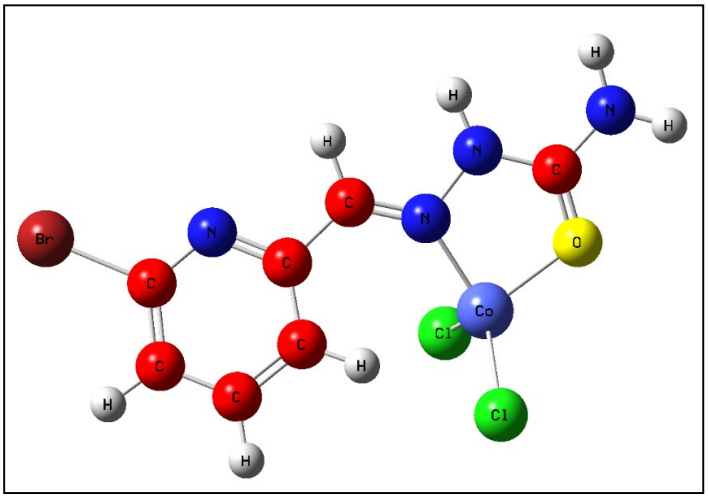
H
H
N
H
N
C
H
C
N
Br
N
C
O
C
Co
C1
C
C
H
C
H
C1
H

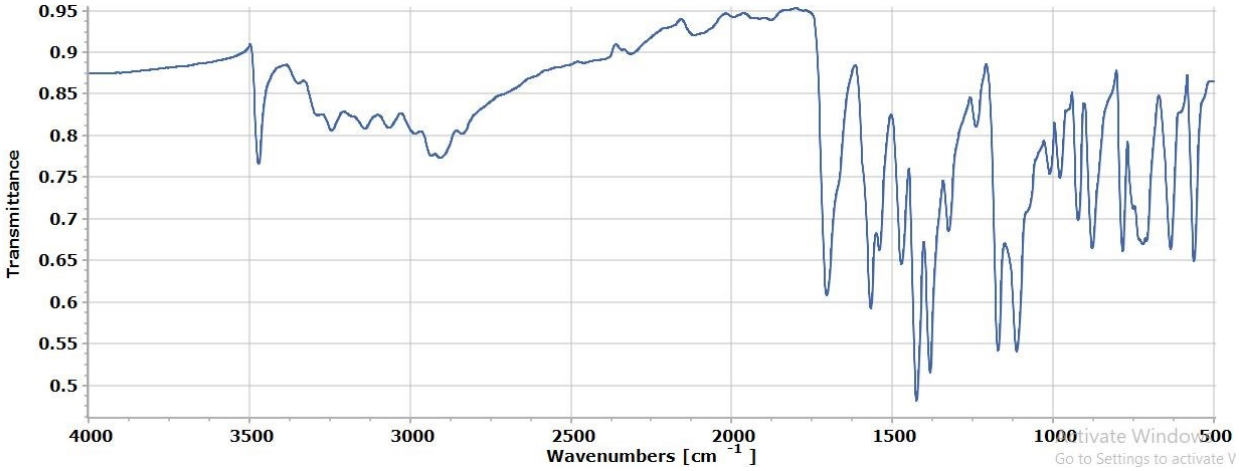
Transmittance
0.95
0.9
0.85
0.8
0.75
0.7
0.65
0.6
0.55
0.5
4000
3500
3000
2500
2000
1500
1000
500
Wavenumbers [cm -1]

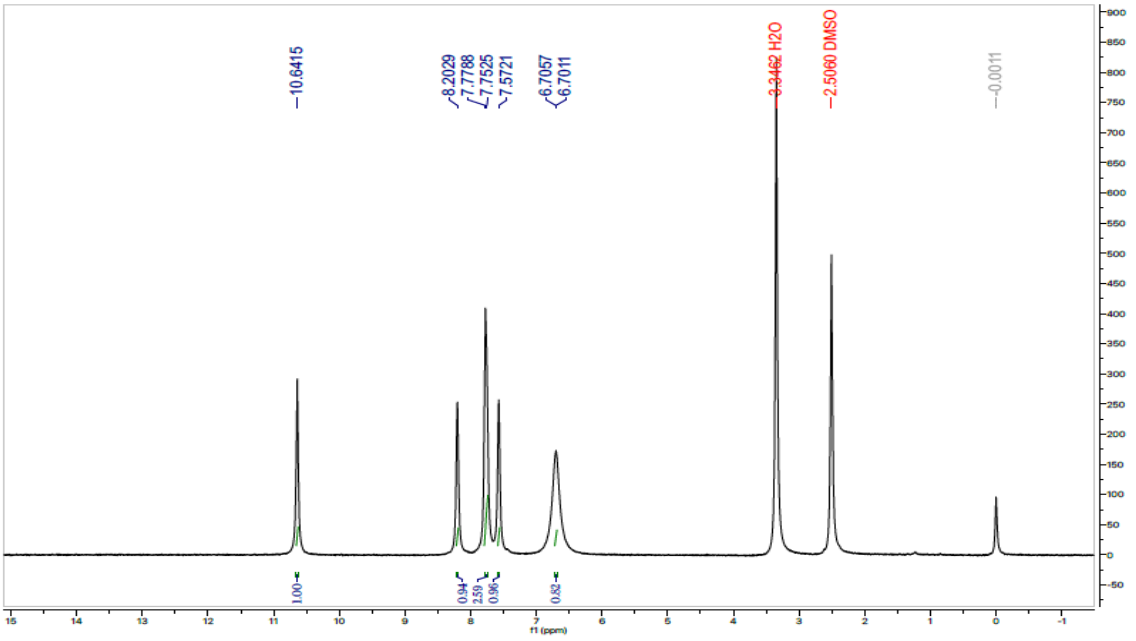
10.6415
8.2029
7.7788
7.7525
7.5721
6.7057
6.7011
3.3462 H2O
2.5060 DMSO
0.0011
1.00
0.94
2.50
0.96
0.82
f1 (ppm)

CoRx-11-Cl2

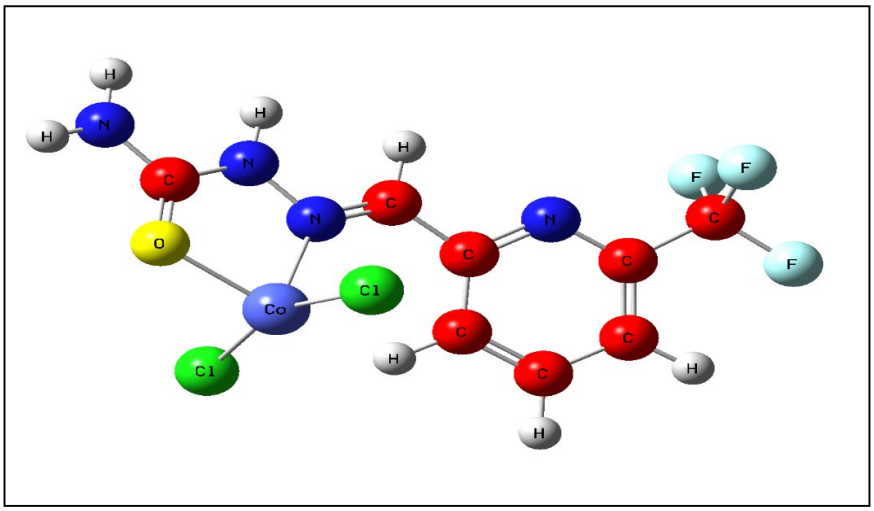
H
N
H
H
N
C
O
N
C
H
C
N
C
C
F
F
C
F
Co
Cl
Cl
C
C
H
C
H
H

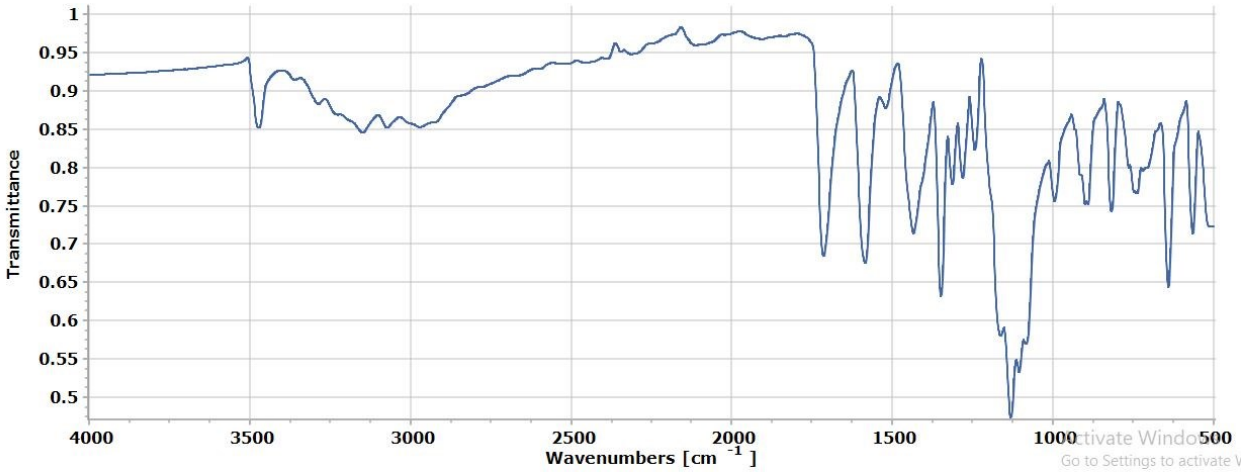
Transmittance
1
0.95
0.9
0.85
0.8
0.75
0.7
0.65
0.6
0.55
0.5
4000
3500
3000
2500
2000
1500
1000
500
Wavenumbers [cm -1]

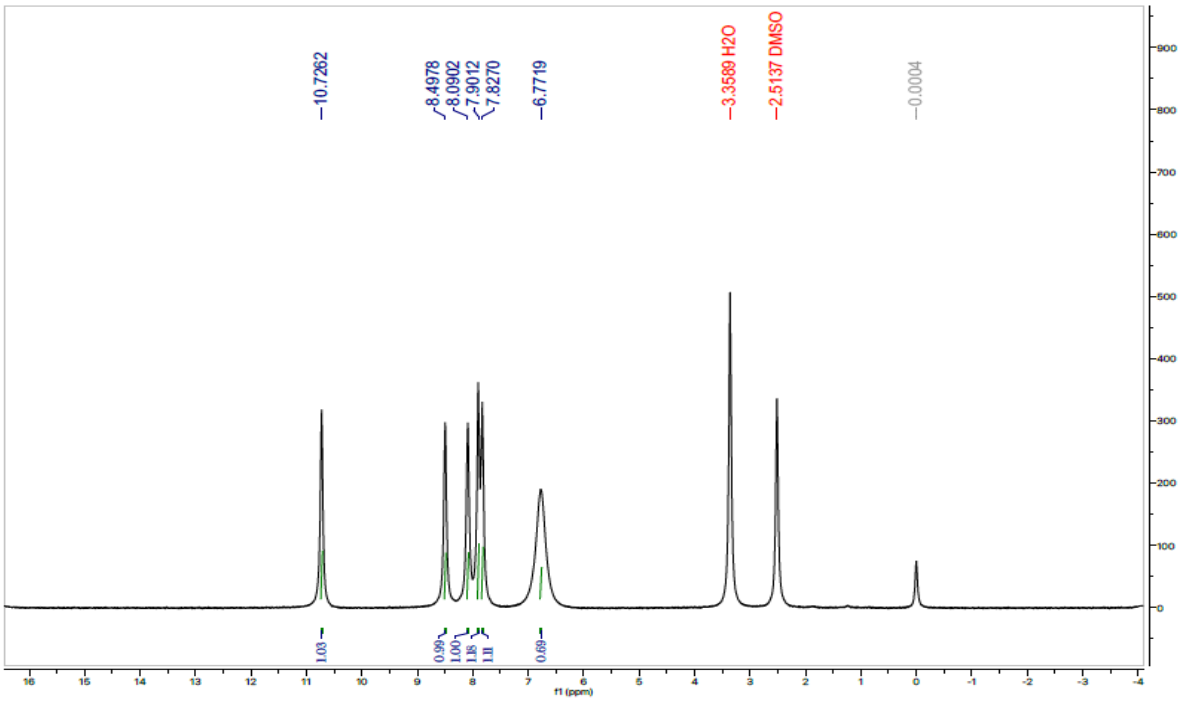
10.7262
8.4978
8.0902
7.9012
7.8270
6.7719
3.3589 H2O
2.5137 DMSO
0.0004
1.03
0.98
1.00
1.85
1.11
0.69
f1 (ppm)

CoRx-12-Cl2

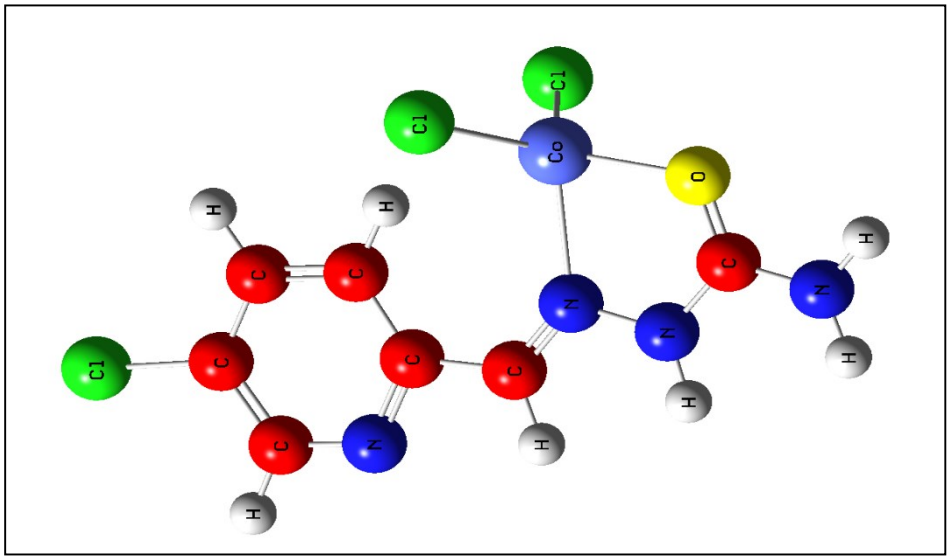
Cl
Cl
Co
O
H
C
N
H

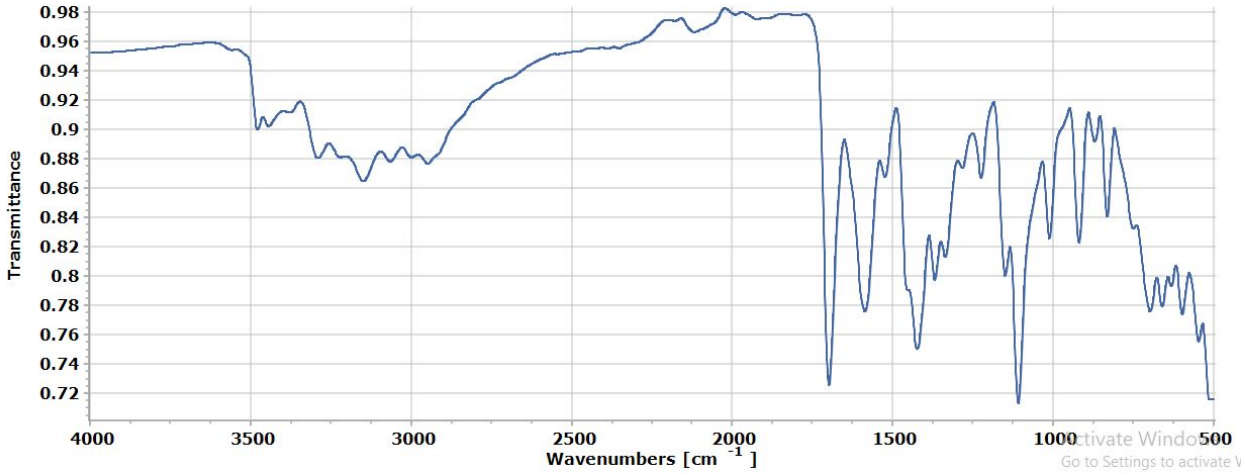
Transmittance
0.98
0.96
0.94
0.92
0.9
0.88
0.86
0.84
0.82
0.8
0.78
0.76
0.74
0.72
4000
3500
3000
2500
2000
1500
1000
500
Wavenumbers [cm -1]

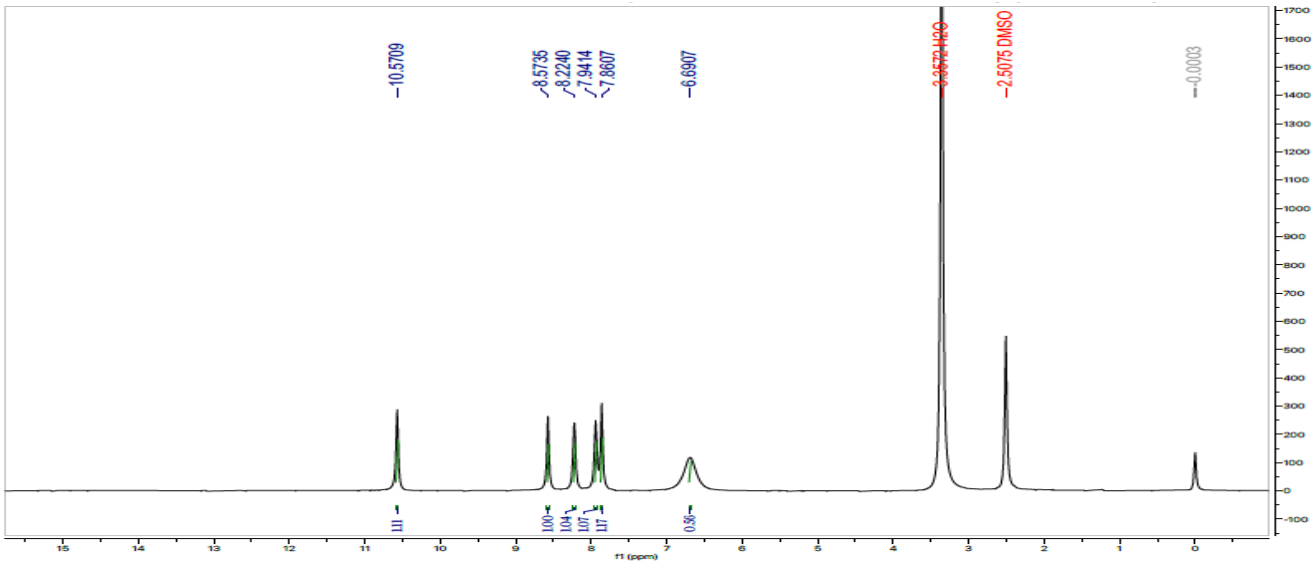
10.5709
8.5735
8.2240
7.9414
7.8607
6.6907
3.5671 H2O
2.5075 DMSO
0.0003
1.11
1.00
1.04
1.07
1.17
0.36
f1 (ppm)

AFM images of nano-sized cobalt complexes of pyridine carboxaldehyde

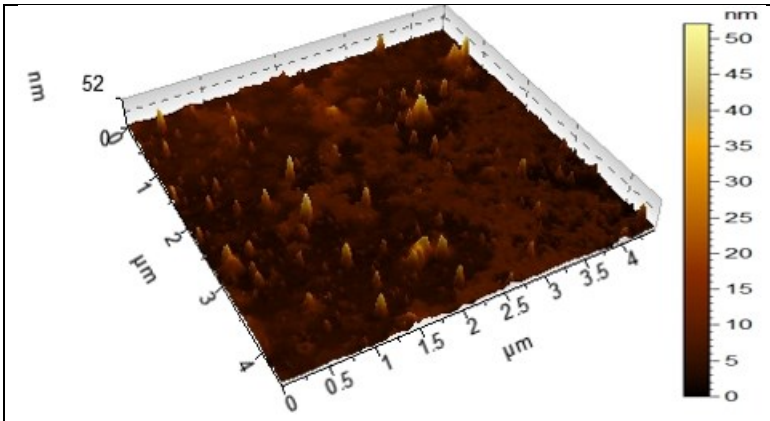

CoRx-1Cl₂

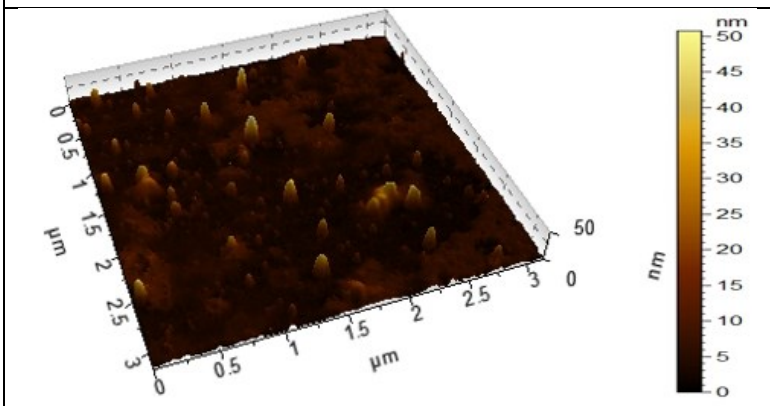

CoRx-3Cl₂

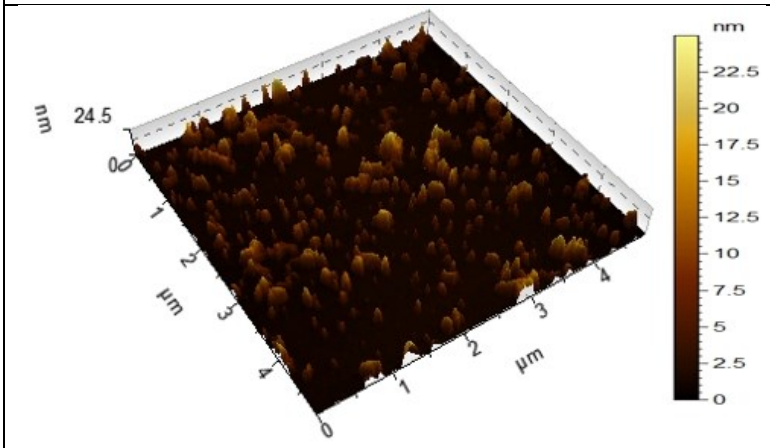

CoRx-4Cl₂

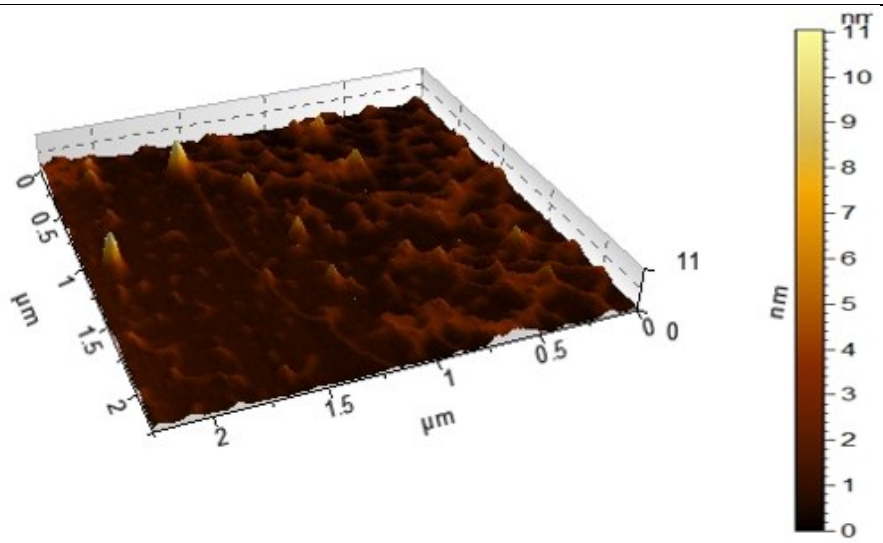

CoRx-5Cl₂

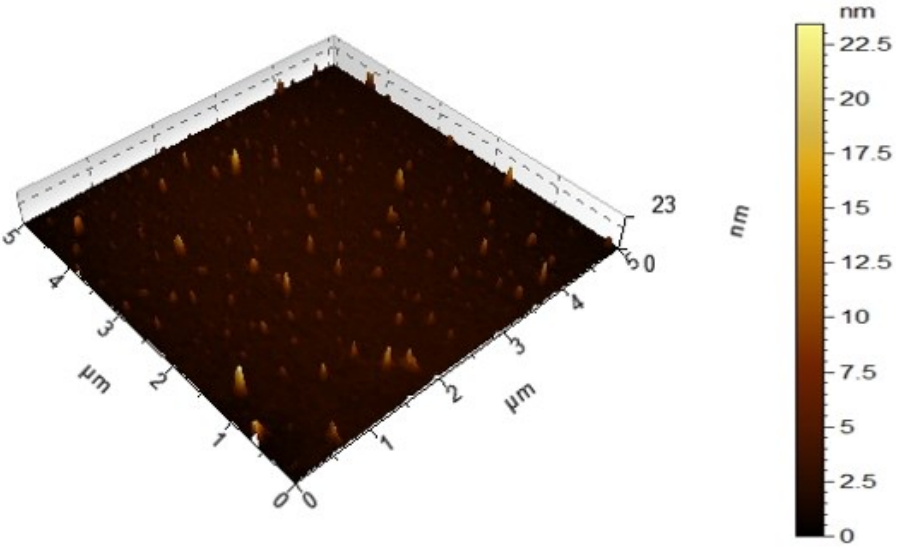

CoRx-6Cl₂

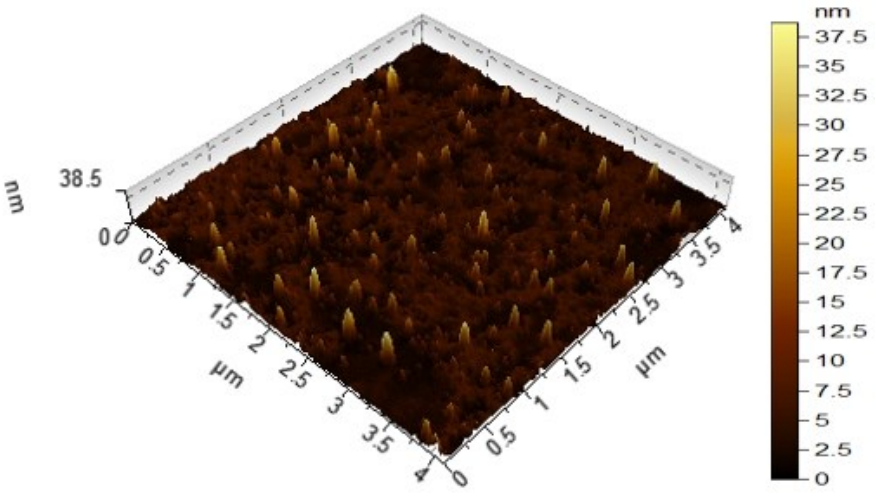

CoRx-8Cl₂

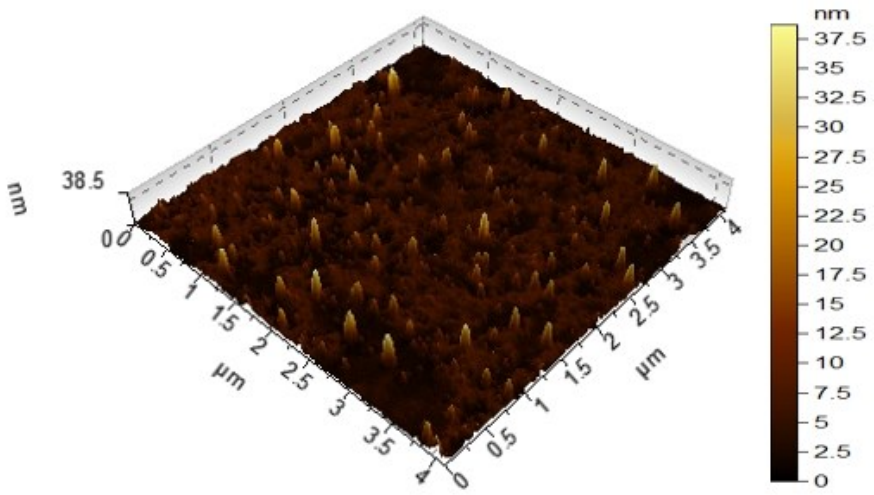

CoRx-8Cl₂

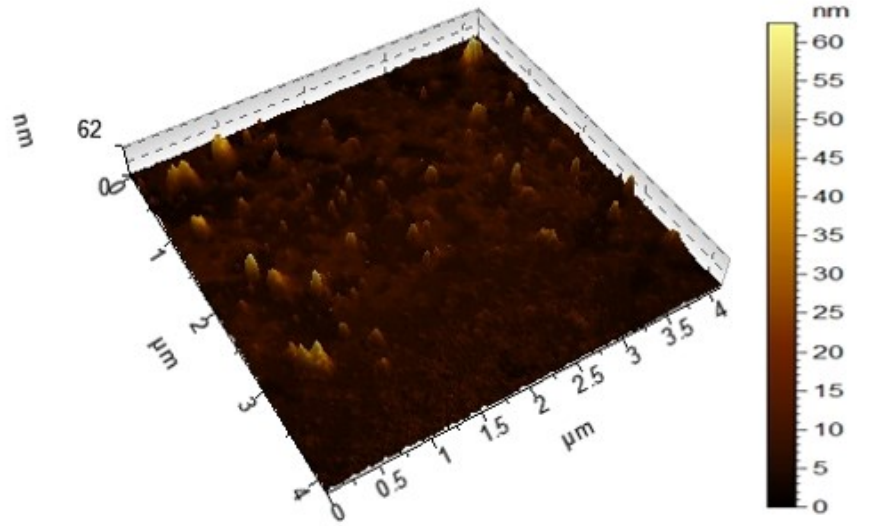

CoRx-9Cl₂

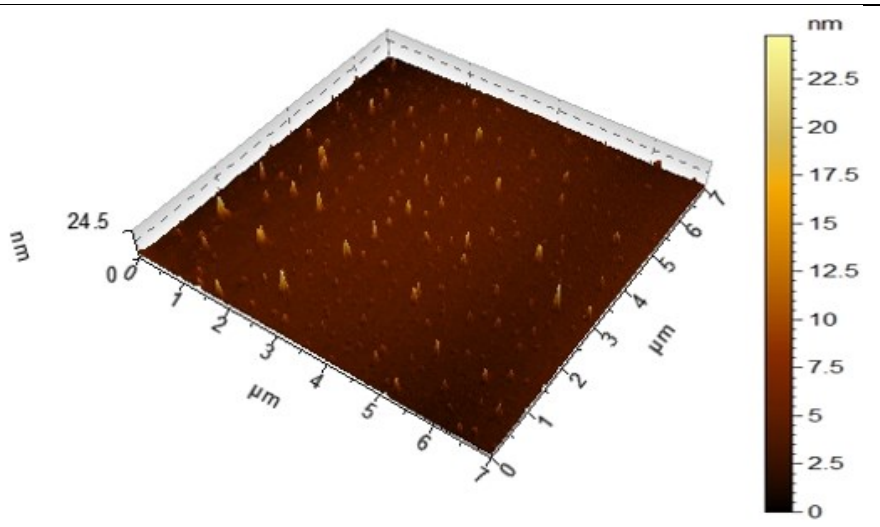

CoRx-11Cl₂

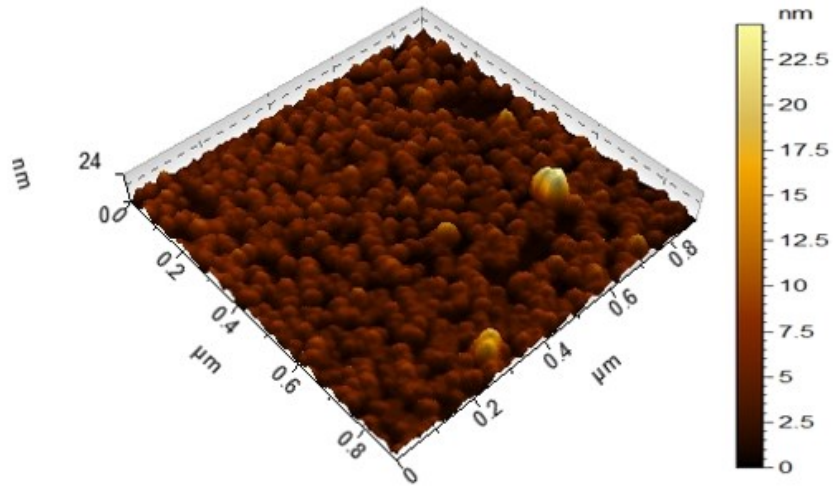

CoRx-12Cl$_2$